STC Technical Report 3333

Continuation of the NVAP Global Water Vapor Data Sets for Pathfinder Science Analysis

Thomas H. Vonder Haar
Science and Technology Corporation
Fort Collins, Colorado

With Contributions from:
John M. Forsythe
Darren McKague
David L. Randel
Benjamin C. Ruston
Shannon Woo
Science and Technology Corporation
Fort Collins, Colorado

Prepared for
National Aeronautics and Space Administration
Goddard Space Flight Center
As Final Report
Under Contract No. NASW-00032

October 2003

Science and Technology Corp.
10 Basil Sawyer Drive, Hampton, VA 23666-1393

…An Innovative Advanced Technology Company

FOREWORD

Science and Technology Corporation is pleased to submit this final report entitled "Continuation of the NVAP Global Water Vapor Data Sets for Pathfinder Science Analysis" by Dr. Thomas H. Vonder Haar. The work was performed under Contract No. NASW-00032 from NASA Goddard Space Flight, Greenbelt, Maryland.

Drs. Thomas Greenwald, Richard Engelen, and Graeme Stephens made special contributions to the NASA Water Vapor Project (NVAP) via their independent research and discussions with the NVAP team. Dr. Arnold Gruber at NOAA/NESDIS provided valuable help to obtain the ATOVS sounding product data. Thanks to Dimitri Chappas and Axel Graumann of the National Climate Data Center for assistance with obtaining the ATOVS data. Joel Susskind, Jeffrey Whiting and Lena Iredell at NASA Goddard provided the TOVS Pathfinder Path A data. Brian Soden at Geophysical Fluid Dynamics Laboratory assisted with the TOVS data. Tropical Rainfall Measuring Mission (TRMM) Microwave Imager data are produced by Remote Sensing Systems and sponsored by NASA's Earth Science Information Partnerships (ESIP): a federation of information sites for Earth Science; and by NASA's TRMM Science Team.

CONTENTS

Page

LIST OF FIGURES

Page

LIST OF TABLES

Page

1. INTRODUCTION

The NASA Water Vapor Project (NVAP) began in the early 1990s as a NASA pilot Pathfinder project designed to measure the distribution of Earth's water vapor from satellite. NVAP is a valuable dataset to address several key NASA Earth science questions which have been listed by Asrar et al. (2001), such as "how is the global cycling of water changing?" and "how well can long-term climatic trends be predicted or assessed?" Climate Data Records (CDR) from NVAP build a foundation for research and understanding of variability of Earth's water cycle on timescales from days to decades (Vonder Haar et al., 2003). NVAP products have been used for a variety of purposes such as model validation, understanding the dynamics of the monsoon, and solar energy calculations. NVAP data now cover the period 1988–2001 (Forsythe et al., 2003). NVAP results have been referenced in more than 75 refereed publications to date, and the consistency of the dataset has been independently verified by Simpson et al. (2001). Two presentations (Vonder Haar et al., 2003 and Forsythe et al., 2003) on the NVAP dataset were presented at the 12th American Meteorological Society Conference on Satellite Meteorology and Oceanography in February 2003.

This report covers the extension of the NVAP dataset into data years 2000 and 2001. This latest phase of NVAP is called NVAP-Next Generation (NVAP-NG). It was a 3-year effort from 2000 to 2003. The products delivered to the NASA Langley Distributed Active Archive Center (DAAC) all fall under the umbrella name of NVAP and now span the time period 1988–2001. Several interesting climate events have been captured in NVAP including the eruption of Mt. Pinatubo in 1991 and the major El Niño of 1997–1998. Production of the initial years of NVAP is described in Randel et al. (1996) and Vonder Haar et al. (1995).

The products created during NVAP-NG have been delivered to the NASA Langley DAAC and are available via the Internet at: **http://eosweb.larc.nasa.gov/PRODOCS/nvap/table_nvap.html**. This report documents the techniques used to create the products, and shows some early science results.

An important contribution of this work was the delivery of data years 1998 and 1999 to the NASA DAAC, using the same NVAP production techniques as in the previous efforts. This data has begun to appear in refereed scientific publications.

A new NVAP CD-ROM with animations and metadata has been created, covering 1988 through 1999 data. It has been distributed to select NVAP users. It is expected that it will be mass-produced and made available via the GEWEX (Global Energy and Water Cycle Experiment) project office in the second half of 2003.

The phase of NVAP we describe here is not simply an extension of previous methodologies and datasets to extend the time record. Rather, increases in computer power and satellite sensors have been tapped to create new NVAP products that maintain continuity with the past, while increasing the spatial and temporal resolution of the products.

In order to provide a context for the NVAP-NG efforts, it is important to remember the history of NVAP. Figure 1 shows the evolution of the NVAP dataset through time, including the years 2000 and 2001 covered here. NVAP-NG builds upon the successful foundation of NVAP. With any satellite-derived CDR, there exists the issue of seamlessly merging new sensors and algorithms to create a product that is consistent in time. Removal of these algorithm changes is a reason to consider reanalysis of the entire NVAP dataset (Suggs and Jedlovek, 2001), but such work is beyond the scope of the NVAP-NG project discussed here. We employed the concept of a "bridge" period as part of our NVAP-NG efforts, to compare the heritage and NVAP-NG approaches, and the results are shown in Section 6.

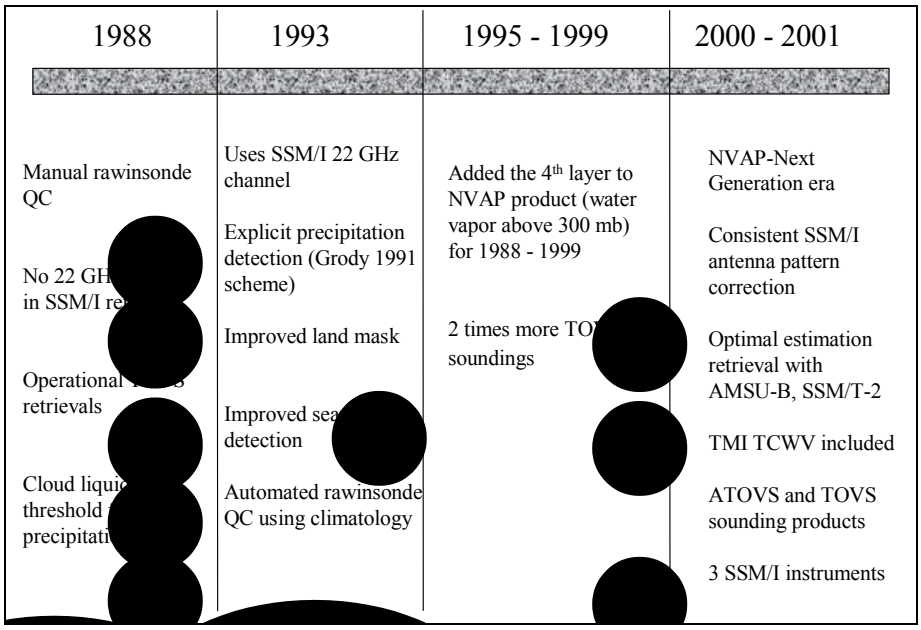

Figure 1. Chronology of modifications to data content and processing of NVAP, including the years 2000 and 2001 discussed here. See Appendix D for discussion of time-dependent biases.

The major differences between NVAP and NVAP-NG are shown in Figure 2. It is readily apparent that NVAP-NG represents an enhancement in every aspect of product generation, i.e., greater number of sensors input, greater spatial and vertical resolution, and more output products and diagnostics.

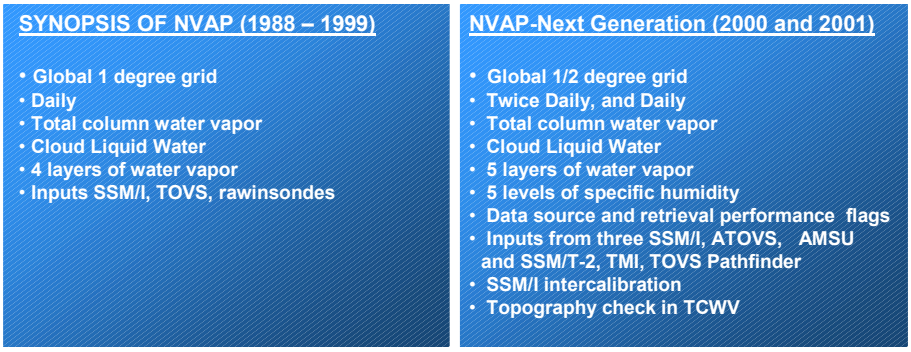

Figure 2. Comparison of NVAP and NVAP-NG. With more satellite inputs and higher spatial / temporal resolution, NVAP-NG (2000–2001) adds to the existing NVAP (1988–1999) to create a 14-year, continuous high quality global water vapor dataset.

An important use of NVAP data is in general circulation model (GCM) validation. A design philosophy of NVAP-NG is to make it independent of forecast model data. For instance, in NVAP-NG we create our own atmospheric temperature profile from available satellite data rather than using model temperature fields such as from the NCEP Reanalysis.

Consistency with the past is essential in order to monitor Earth's water vapor fluctuations on timescales greater than decades. With the plethora of satellite instruments becoming available beyond 2001, including the NASA Aqua platform, our ability to measure Earth's water vapor will continue to improve.

2. INPUT DATA

NVAP-NG utilized a wide variety of satellite sensors, much more than in any previous NVAP production year. Figure 3 shows the time periods covered by the sensors used during NVAP-NG. Note that a few sensors (TOPEX, MODIS) were withheld, allowing valuable intercomparisons in the future such as performed by Simpson et al. (2001). We used a variety of feeds to acquire the data (Table 1). We detail in this section more specifically some aspects of the data treatment.

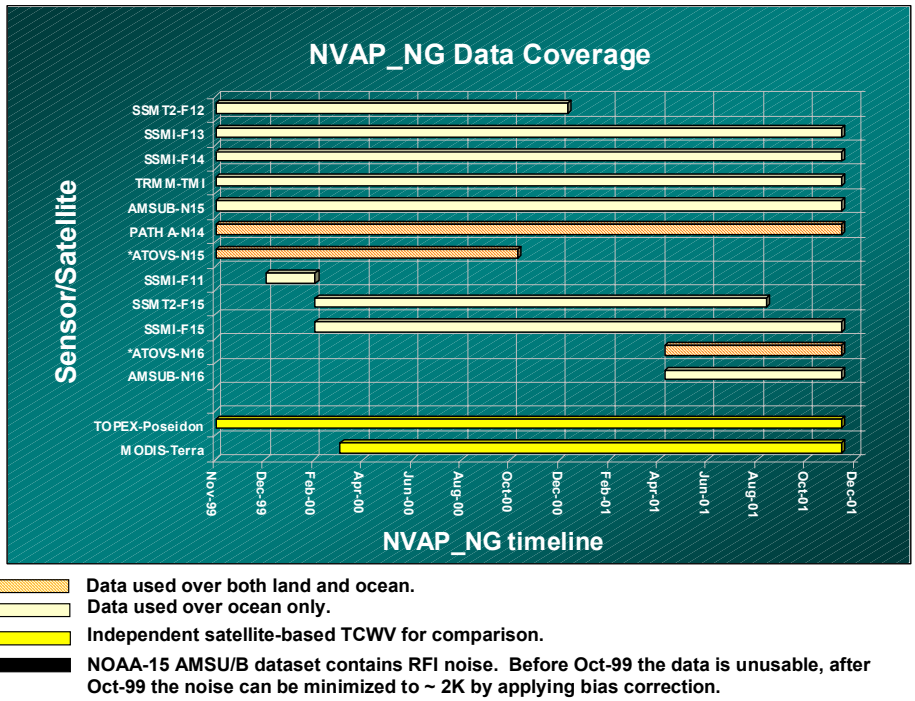

Figure 3. NVAP-NG combines a changing cast of over 10 polar-orbiting instruments to create a global water vapor dataset.

Table 1. Datasets and Sources Used in NVAP-NG Project

DATASET	SOURCE
SSM/I	NOAA Satellite Active Archive (SAA) (Internet)
AMSU-A/B	NOAA SAA and CIRA via tape
SSM/T-2	NOAA SAA
ATOVS Soundings	NCDC via Internet
TOVS Pathfinder Reanalysis	GSFC via Internet
Sea Surface Temperature and Sea Ice Data	NOAA
TMI Products	Remote Sensing Systems via Internet
Topography	NOAA ETOPO5

Microwave Radiances

The backbone of NVAP is the microwave radiances from SSM/I and AMSU. Figure 4 shows an example of brightness temperatures from AMSU-B. A key component of our treatment of the microwave data was the application of an updated antenna pattern correction to the SSM/I data (Colton and Poe, 1999). This reduces the intersatellite biases in retrievals due to slight differences in the SSM/I instruments onboard the DMSP spacecraft. Overall, the correction causes a few tenths of a millimeter increase in the global average of total column water vapor (TCWV). Further details on this correction are shown in Forsythe et al. (2003).

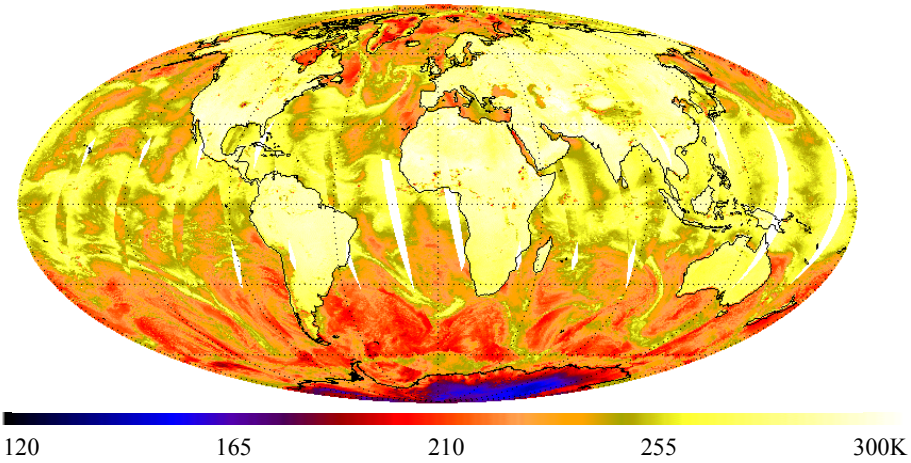

Figure 4. Example of a raw radiance input, in this case the AMSU/B 89 GHz brightness temperatures from July 1, 2000. The OE retrieval is run on a combination of AMSU/A and AMSU/B channels to retrieve the water vapor profile.

The NOAA-15 instrument has a known problem with Radio Frequency Interference (RFI) (Atkinson, 2001). Correction of this problem is quite complex and is time-dependent. Our original source of AMSU-B data (HDF-EOS format from NESDIS) did not contain sufficient information to implement the correction. Knowledge of the vehicle transmitter configuration and telemetry in raw counts was required. The solution was to download Level 1b data from the NOAA Satellite Active Archive (SAA) system from November 1999 through December 2001. This is the raw form that allows corrections to the counts to be made. A Level 1b decoder was written to apply the corrections and create new sets of brightness temperatures. The AMSU-B data can be considered unusable for our retrievals prior to October 1999 because of the transmitter configuration (Atkinson, 2001). Dynamic bias corrections were developed after that date which allow noise reduction to less than 2 K. Figure 5 shows a before and after RFI correction image and the amount of correction being applied.

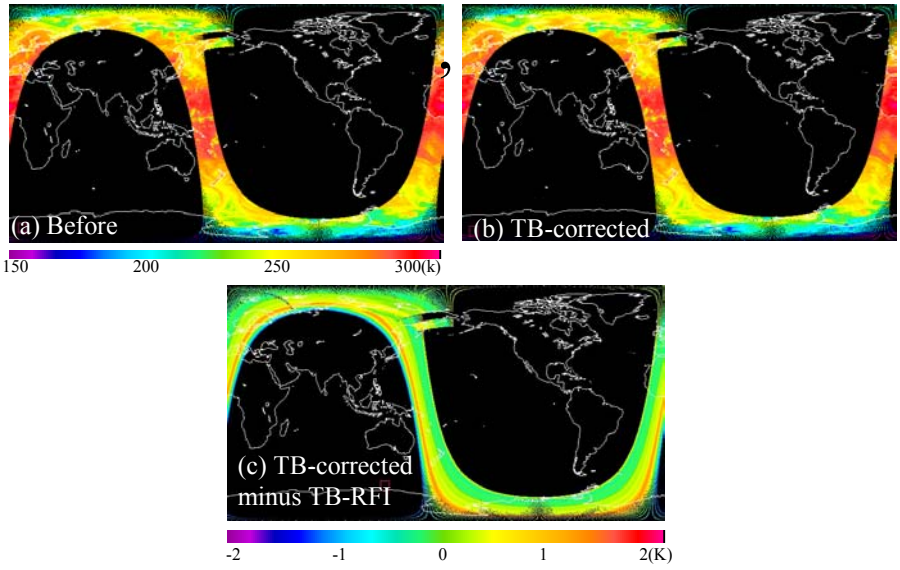

Figure 5. Sample orbital image of NOAA-15 AMSU-B RFI correction from May 18, 2000. 150 GHz brightness temperature (a) before correction (b) after correction (c) amount of correction applied (in Kelvin).

3. SATELLITE RETRIEVAL PRODUCTS

STC-*METSAT* performs retrievals on the AMSU, SSM/T-2, and SSM/I data. TRMM Microwave Imager (TMI), ATOVS, and Pathfinder Path A retrievals are performed externally, and the products are brought into STC-*METSAT* to merge into the final dataset. Figure 6 shows examples of these fields before they are brought into the final merge. The ATOVS products are those described in Reale (2001), the Pathfinder Path A are from Susskin et al. (1997), and the TMI results are from Remote Sensing Systems (available via the Internet at www.ssmi.com).

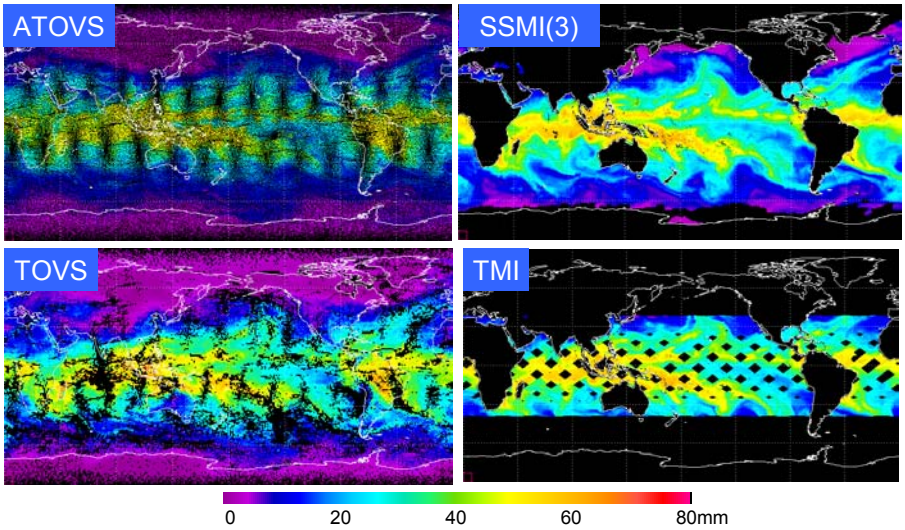

Figure 6. A sample of satellite retrieval products. Images from January 1, 2000 showing ATOVS, Pathfinder Path A TOVS, SSM/I (3 instruments) and TMI.

Ancillary Data

STC-*METSAT* employed several static or slowly changing datasets to support the NVAP-NG production. An example of each of these is shown in Figures 7 and 8. In Figure 7, the topography and sea ice fields are shown. Topography is from the ETOPO5 global dataset, and the sea ice fields are supplied with the sea surface temperature (SST) data (Reynolds et al., 2002). An example of the Reynolds SST field is shown in Figure 8c. The daily cloud liquid water field, the daily wind speed field, and the daily temperature profile fields were created from radiances at STC-*METSAT*. These fields are needed for the AMSU and SSM/T-2 optimal estimation (OE) retrieval as first guesses. The wind speed and cloud liquid water are products of the SSM/I retrieval (Greenwald et al., 1993), and the temperature fields are from the statistical AMSU retrieval of Goldberg described in Kidder et al. (2000).

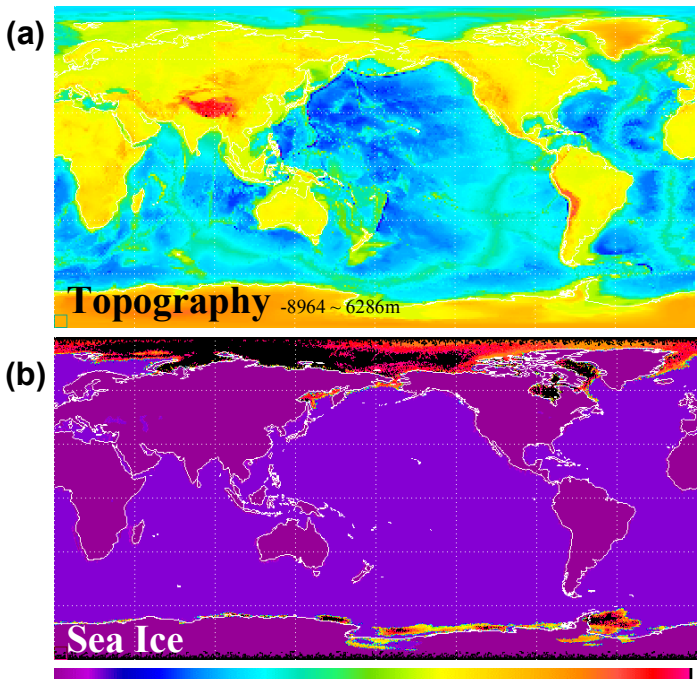

Figure 7. **Ancillary data used in NVAP-NG. (a) Half-degree topography map created from NOAA ETOPO5 dataset. (b) Sea ice (red and yellow areas) from NOAA Reynolds Version 2 dataset.**

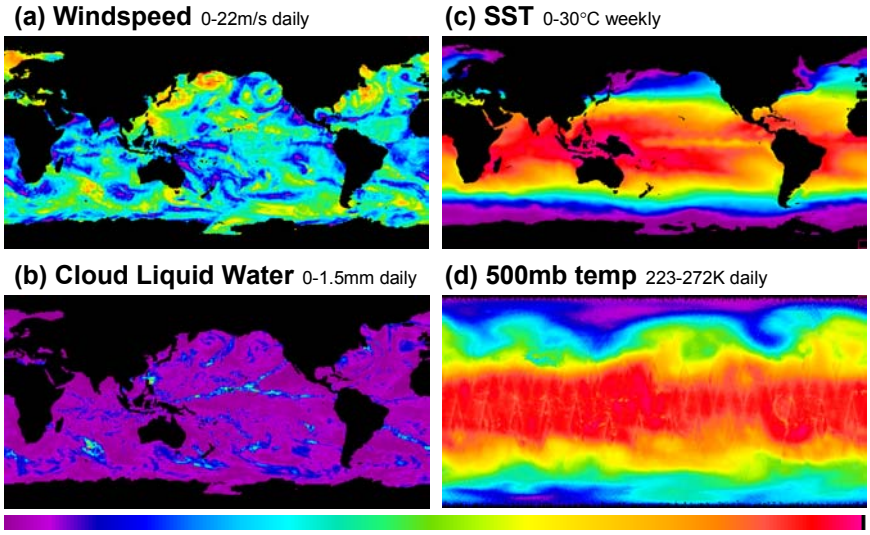

Figure 8. **Ancillary data example from January 20, 2000. Wind speed and cloud liquid water are from our SSM/I retrieval. Sea surface temperature data are from the Reynolds dataset (Reynolds et al., 2002). 500 mb temperature is from Goldberg's AMSU-A retrieval described in Kidder et al. (2000).**

4. RETRIEVAL ALGORITHMS

A major accomplishment during NVAP-NG was the implementation of an optimal estimation (OE) retrieval to retrieve water vapor profiles from AMSU and SSM/T-2. Much development time was spent on this process. An OE retrieval minimizes the differences between the measured and calculated radiances, and the retrieved versus constraint atmospheric state. Figure 9 shows the cost function of the OE retrieval, and a comparison to a NESDIS operational algorithm. The retrieval used here is fashioned after the method of Engelen and Stephens (1998).

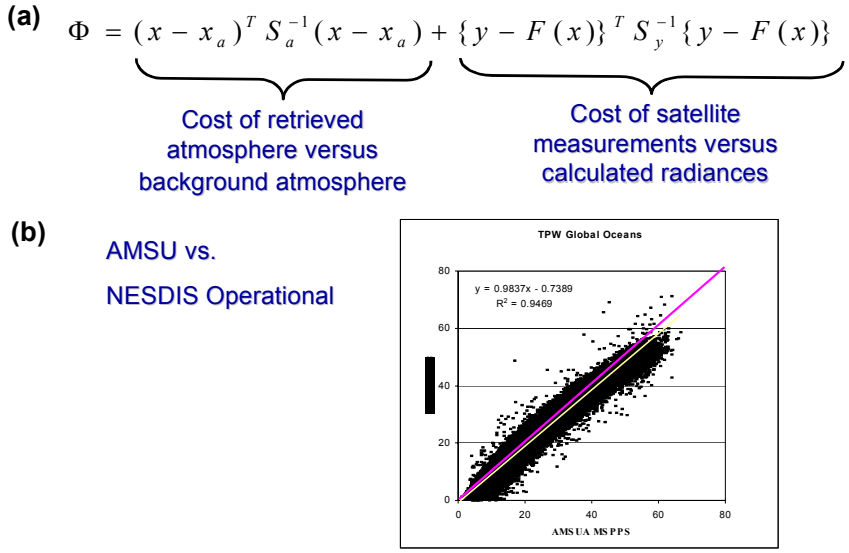

Figure 9. (a) The cost function equation for the passive microwave Optimal Estimation (OE) algorithm. (b) Comparison of OE algorithm derived total precipitable water and NESDIS MSPPS AMSU-A retrieved total precipitable water for September 20, 2000. Correlation is 99%.

Data flow diagrams were created by STC-*METSAT* to orchestrate the flow of data through the OE retrieval. Figure 10 shows the flow of AMSU and SSM/T-2 data. Since AMSU A/B and SSM/T-2 are not identical instruments, some modifications were made in the code to account for their differing channels. In particular, the SSM/T-2 retrieval was not allowed to iterate on the first guess temperature profile, since it had no 50–60 GHz temperature sounding channels. The stratospheric temperature channels (> 55 GHz frequency) of AMSU-A were not used in the retrieval since they had no impact on the water vapor retrieval results. The NOAA-15 AMSU-B channels were given an instrument noise value of 2 K, in accordance with the reduction in RFI expected from Atkinson (2001). Figure 11 shows examples of the AMSU and SSM/T-2 TCWV retrievals.

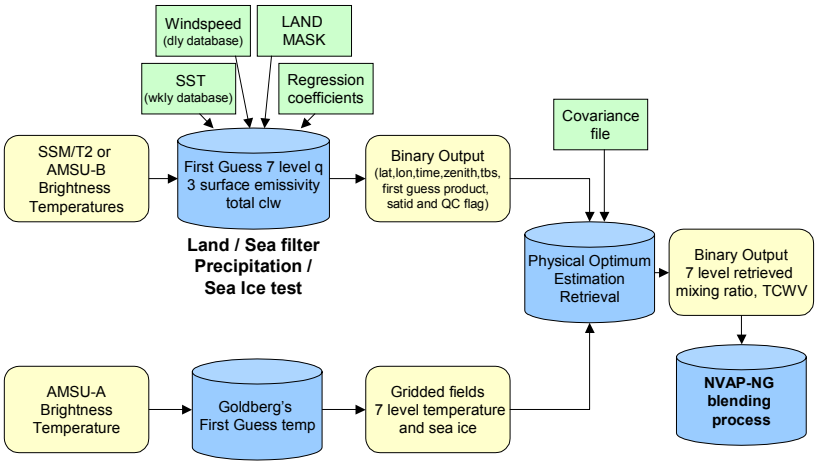

Figure 10. Flow of the AMSU-B and SSM/T-2 data through the retrieval process.

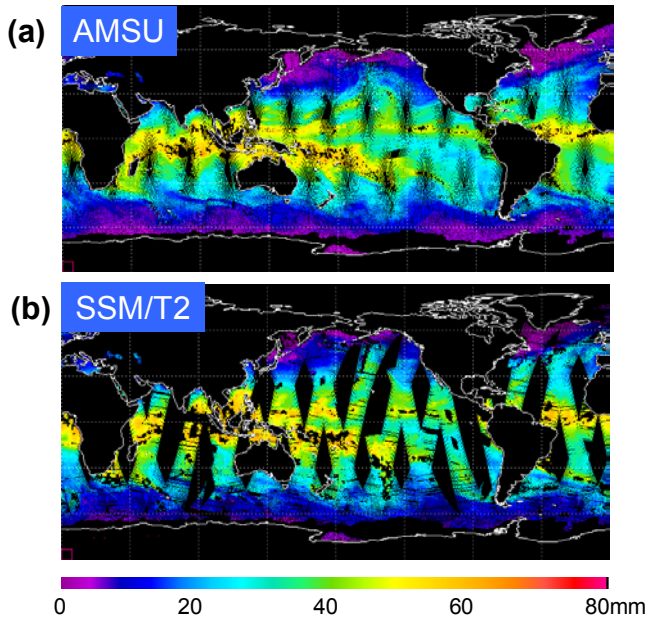

Figure 11. OE TCWV retrieval sample product from January 1, 2000. (a) NOAA 15 AMSU (b) SSM/T-2.

The SSM/I retrieval was essentially unchanged from previous NVAP efforts, except for the new antenna pattern correction and improved land detection. Figure 12 shows the flow of data through the SSM/I retrieval. Table 2 summarizes the two retrievals.

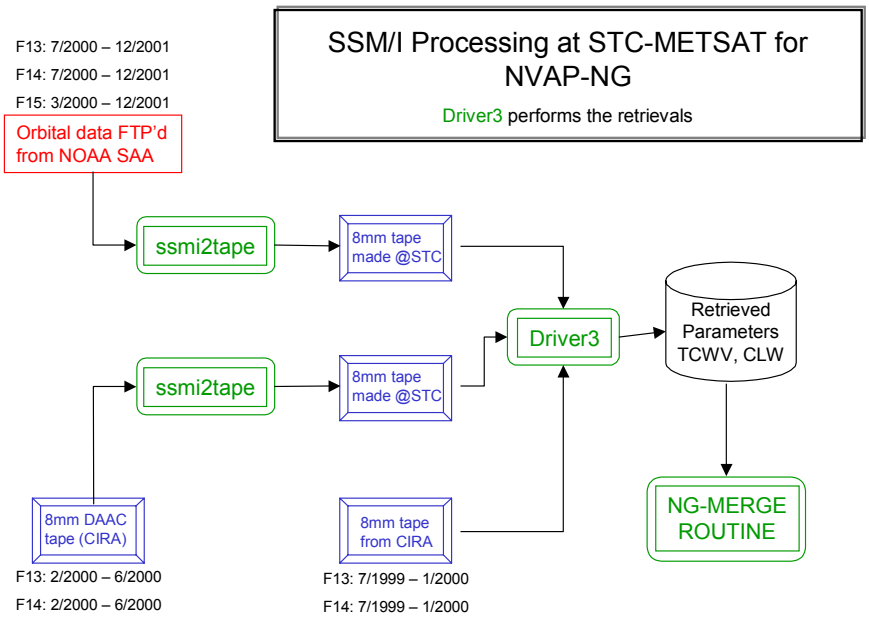

Figure 12. Flow of SSM/I data to retrieve total column water vapor and cloud liquid water.

Table 2. Retrievals Performed at STC-METSAT

Instrument	Retrieval Algorithm
SSM/I	Physical retrieval of Greenwald et al. (1993). Same as used in previous NVAP production but with Antenna Pattern Correction results of Colton and Poe applied.
AMSU A/B	Optimum estimation method of McKague et al. (2001). Ocean only. First guess windspeed and cloud liquid water supplied from SSM/I retrieval. SST first-guess from Reynolds weekly values. Water vapor profile first-guess from monthly average of 12 previous years of NVAP.

5. BLEND PROCEDURE

We use a weighted blending scheme to bring our diverse satellite water vapor column and profile measurements together. This approach was modeled after the Global Precipitation Climatology Project (GPCP) technique of Huffman et al. (1995).

Figure 13 outlines the process, which can be likened to a series of shells. The outermost shell is the input and pre-conditioning of the satellite data. Retrievals are then run, and the results are blended together. Extensive quality control occurs at each shell, and is described in detail in this section. The ultimate goal is delivery of high-quality science data to science users to study atmospheric and hydrologic processes involving water vapor.

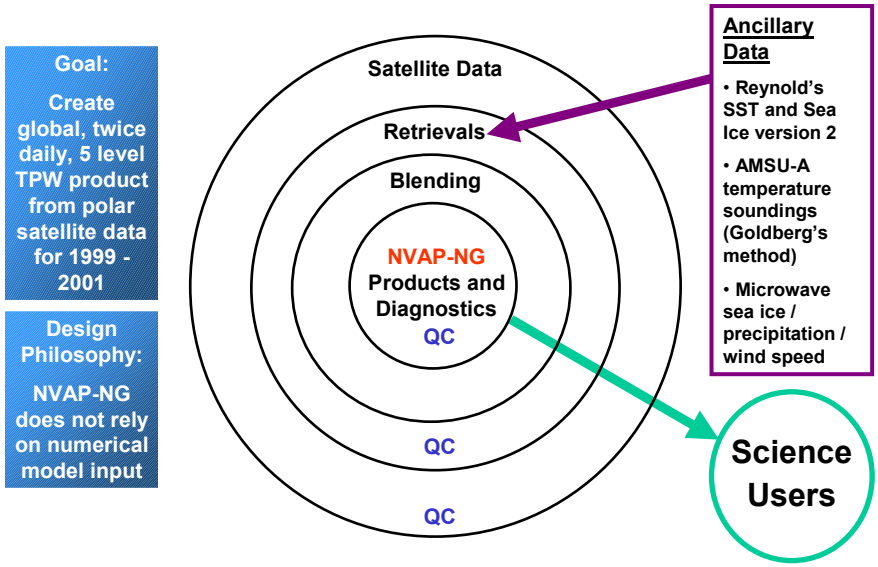

Figure 13. "Shell" concept of NVAP-NG. Raw and ancillary data are run through retrievals and blended with intermediate products to create the NVAP-NG fields. Quality control is performed at each level. The blended products then go to the science community.

The fields created in NVAP-NG are listed in Appendix A. Figure 14 shows how these products are created and relate to each other. NVAP before 2000 carried layered precipitable water (PW) in four layers only. In contrast, NVAP-NG carries layered PW, and mixing ratio on five pressure levels. The process for how the fields are merged is now discussed in more detail.

5.1 TOTAL COLUMN WATER VAPOR

The values are retrieved from AMSU, SSM/T-2, and SSM/I (ocean only) and ATOVS and Pathfinder Path A (global, except for heavy cloud and precipitation regions). These values are brought together to form the Total Column Water Vapor (TCWV) product. We apply weights in this process, with the SSM/I weighted most heavily. The SSM/I algorithm has been proven to yield good values over the ocean. The weights can be thought of in terms of percent or relative to each other. The weights used for each dataset in NVAP-NG are shown in Table 3. A lower number means a higher weight is applied in the merge.

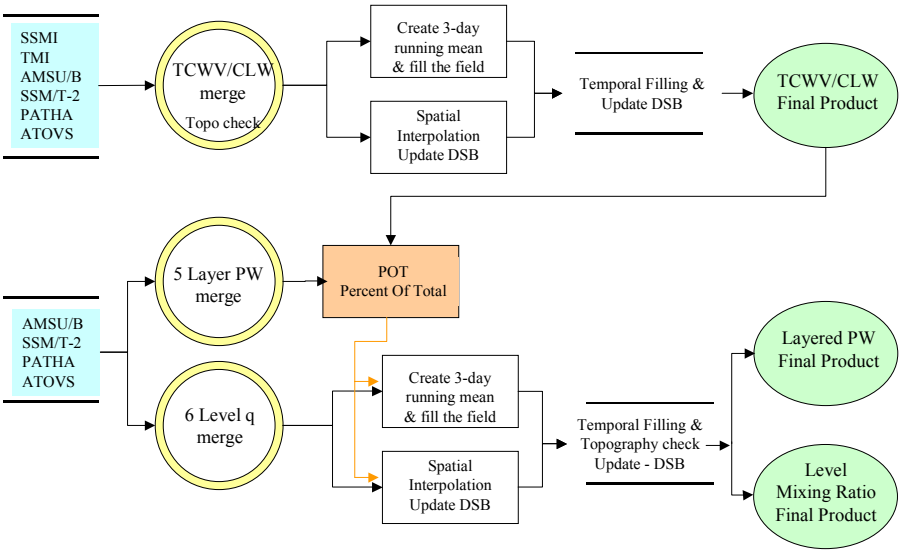

Figure 14. Flow of the NVAP-NG final merge process.

Table 3. Relative Weights for Weighted Blending

RELATIVE WEIGHT (%)	INSTRUMENT
18.0	SSM/I
35.0	Path A TOVS N14
35.0	ATOVS N15
30.0	ATOVS N16
25.0	SSM/T 21st
22.0	AMSU-B N15
20.0	AMSU-B N16
18.0	TMI TRMM

Via this approach, a global TCWV field is created. This field is then input into the layered amount determination.

5.2 LAYERED PRECIPITABLE WATER AND LEVEL MIXING RATIO

The AMSU, SSM/T-2, ATOVS, and Pathfinder Path A results all report mixing ratio (q) on the 1000, 850, 700, 500, 300 and 200 mb pressure surfaces. The q values are not modified or adjusted after the retrieval. A ½-degree topography mask is used to screen out values that are below the ground surface. The q values are needed for follow-on science such as water vapor transport calculations.

SSM/I and TMI are the only instruments that do not retrieve a profile of water vapor. The TCWV values for all the other instruments are simply the sum of the layered PW values. Since SSM/I and TMI only currently retrieve over land, this avoids the problem of high terrain and inconsistencies between the total column and the sum of the layers. In NVAP-NG, the following relations holds true:

TCWV = SUM (Layered PW)

TCWV not equal to SUM of layered PW calculated from q

5.3 PERCENT OF TOTAL CALCULATION APPLIED TO LAYERED PRECIPITABLE WATER

Referring back to Figure 14, note that the TCWV value is determined first by blending the multi-sensor inputs together. This is then applied back to the layered PW values through a concept called Percent of Total. This forces consistency between the TCWV value and the sum of the layers. Consider the sample data in Table 4.

Table 4. Example of Applying Percent of Total

Layer	Layered amounts	TCWV = 30 mm	
		% of sum of layers	Final Value
1000-850	10 mm	40	12 mm
850-700	7 mm	28	8.4 mm
700-500	4 mm	16	4.8 mm
500-300	3 mm	12	3.6 mm
300-200	1 mm	4	1.2 mm
Sum	25 mm	100 %	30 mm

The TCWV merge gave a value of 30 mm, but the sum of the layers after merge was only 25 mm, since SSM/I and TMI do not give layer information. The initial layered PW values are scaled to sum up to the TCWV value.

Assume the surface for the data in Table 4 was at 800 mb. Then the results would change as follows: The layered PW and q values for the 1000–850 mb layer would be reported as missing. The layered PW and q values for the 850–700 mb level would be reported unchanged. The TCWV value would be calculated with values from 850 mb to 200 mb, and the percent of total calculation would proceed as above.

5.4 SPATIAL AND TEMPORAL INTERPOLATION

Some sample merge products are shown in Figure 15. During the blend, maps are kept of the number of data points in each grid box. Figure 15d shows an example from January 1, 2000. Note that a data point is considered to be a retrieval from an instrument, not a satellite itself. So for example, NOAA-15 could add data points from the AMSU retrievals as well as the ATOVS retrievals. The impact of the TMI retrievals is evident in the Tropics. Note the large difference (Figure 15d) between the coverage over land and ocean. This is because the microwave retrievals do not currently perform over land surfaces due to unknown surface emissivity. Extension of the retrievals over land awaits further progress from the research community.

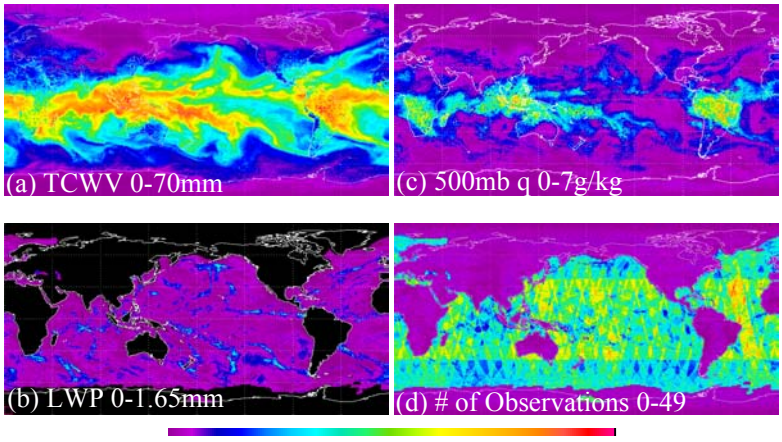

Figure 15. Sample blend final product from January 1, 2000. (a) Total column water vapor (b) liquid water path (c) 500 mb specific humidity (d) number of observations in each grid box.

It is inevitable that some grid boxes will not have coverage in a 24-hour or especially in a 12-hour period. Figure 16 shows the TCWV field for 12 hours on January 1, 2000. Note the black areas, which have

no inputs during that time. In order to fill the grids, we use a multi-pass approach. First, small data-void regions of one or a few pixels are filled with an average of adjacent data. Remaining unfilled points are then handed over to an objective analysis tool (Koch et al., 1983). For any of the few remaining points that have not been filled by these methods, a 3-day running mean temporal interpolation is performed. The data source code table is updated to indicate that the data were interpolated. Figure 16b shows the results of the data interpolation that was applied to Figure 16a.

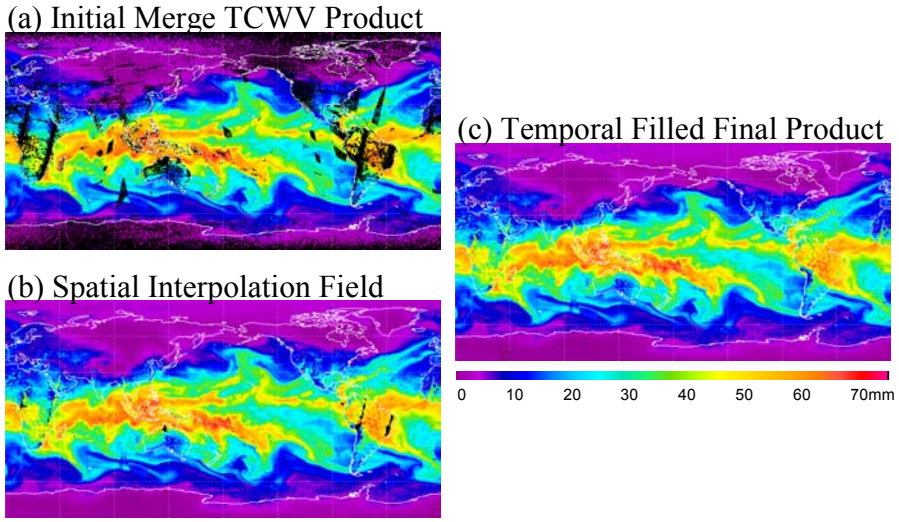

Figure 16. Sample intermediate to final product during filling process from January 1, 2000 0–12 Z. (a) Initial merge TCWV grid, (b) Spatial interpolated field, (c) Temporal filled final product. All filled data are indicated via the data source bit.

We examined a published spatial interpolation method called Kriging, but due to its computational overhead, we decided to use a combination of the distance-weighted Barnes Analysis, neighbor averaging, and temporal persistence. The final temporal-filled field is shown in Figure 16c.

6. QUALITY CONTROL AND PRODUCT INTERCOMPARISONS

6.1 QUALITY CONTROL DURING PROCESSING

Quality controlling the data throughout every step of the NVAP-NG production is one of the most important tasks to create a high quality product. A combination of automated and manual inspections was used. Our approach is to trap as many errors as possible throughout the software without manual intervention. All of our data ingest and reformatting software has extensive quality control tests (e.g., out of bounds values, testing flags indicating instrument problems). Intermediate and final products are examined in the form of 720 x 360 grids.

The following is a list of quality control challenges we encountered beyond those trapped by standard error checking in software, and the solution chosen:

- SSM/T-2 bad data

We manually inspected the brightness temperatures in all channels of the SSM/T-2 data to look for any unusual behavior of the data. In fact, we noted a problem with the calibration of F-15 SSM/T-2 data beginning in September 2001. The slope of the calibration curve per scan line appears to behave erratically at this time. After contacting our colleagues at the Naval Research Laboratory, we determined no alternative source for those four months is available. SSM/T-2 F15 data after September 2001 are not being used in the final product.

The SSM/T-2 F-14 150 GHz channel brightness temperature appeared to be noisy throughout 2000 and 2001. Running retrievals on these data produced noisy results. After examination of the type of retrieved result shown in Figure 17 from the F-14 instrument, we decided to withhold this dataset from the final merge.

- SSM/I bad scan lines

After the SSM/I retrieval has been performed, we visually inspected the 12-hour total precipitable water fields for quality control. We visually inspected the SSM/I merged fields, which include all satellites (F11, F13, F14, F15), and looked for bad scan lines that had crept into the output. F11 has the most frequent occurrence of bad orbits that required remediation. A utility was written that allowed us to specify a time range in minutes and remove those bad scan lines from the particular input satellite. This allowed us to retain as many good data as possible.

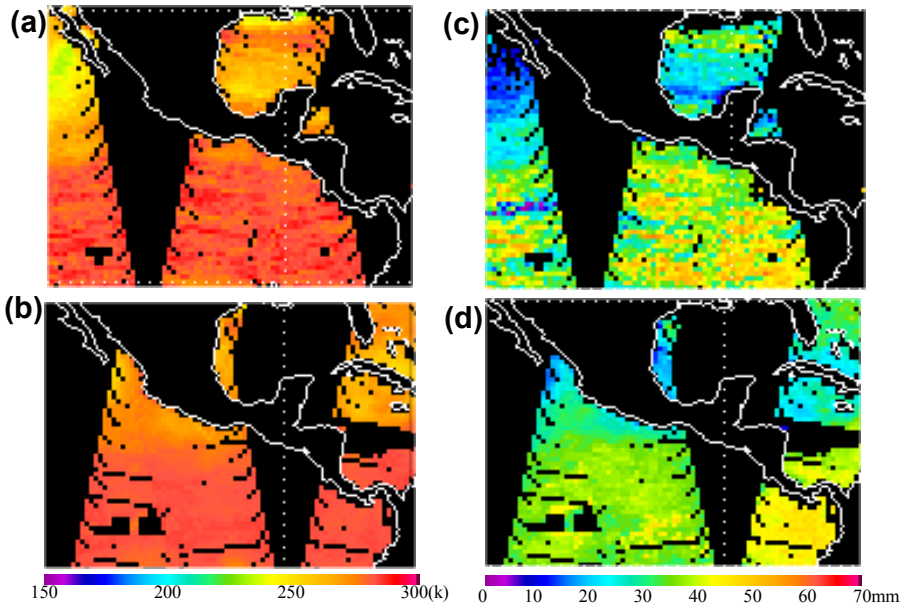

Figure 17. Evidence of DMSP F14 SSM/T-2 bad channel at 150 GHz. Sample image from January 20, 2000. (a) F14 150 GHz TB appear to have noisy pattern throughout the dataset; in comparison F12 (b) does not. As a result, the total column water vapor retrieved from OE method is noisy from (c) F14, but clear from (d) F12.

In total, four satellites at twice per day (roughly 2000 images) were manually inspected. The bad scan removal procedure was applied on a small subset of the total data, roughly 20 minutes per month on average.

SSM/I retrieved products that pass the manual quality control are then used in the final merge. One of our merged products is the standard deviation grid. Using this grid can help identify bad SSM/I scan lines that weren't screened out in the first pass. Figure 18 shows an example. Bad scan lines show up arc-shaped with high standard deviation values and are manually removed. This technique is our second pass in screening the dataset and marking bad scan lines from the SSM/I dataset.

- ATOVS scattered noise (isolated high or low values)

In contrast to the SSM/I bad scan line data, the ATOVS dataset has scattered noise throughout the total and layered precipitable water field. STC-*METSAT* developed a median-type filtering method to correct this. An average of 8000 points per day get screened out, or roughly 6 to 8 percent of the total. The noisy points have an average value of 20 mm difference from the surrounding points. Figure 19 shows some before and after scenes indicating how the median filter eliminates bad ATOVS points.

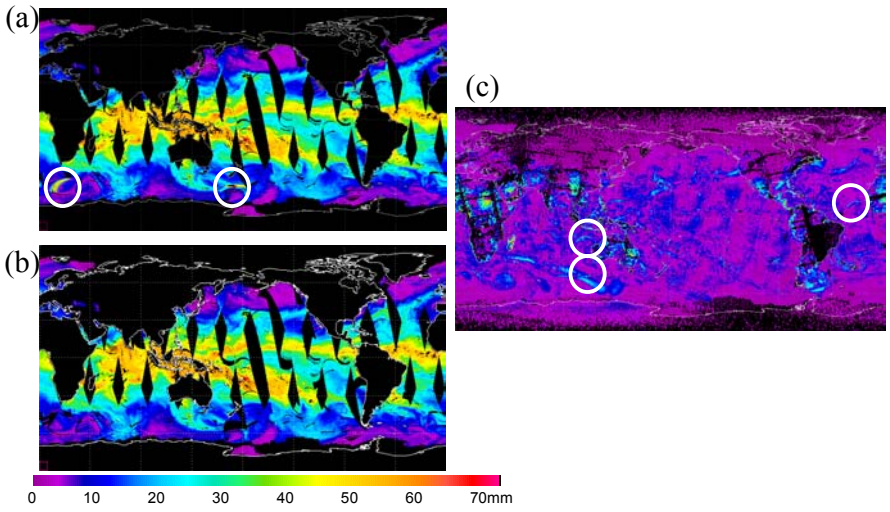

Figure 18. **SSM/I quality control, sample image from January 11, 2000. (a) The first pass is to visually inspect bad scan lines in TCWV field. Bad scan lines are removed in (b). The second pass (c) uses standard deviation grids from the merge output to identify and mark more bad scan lines.**

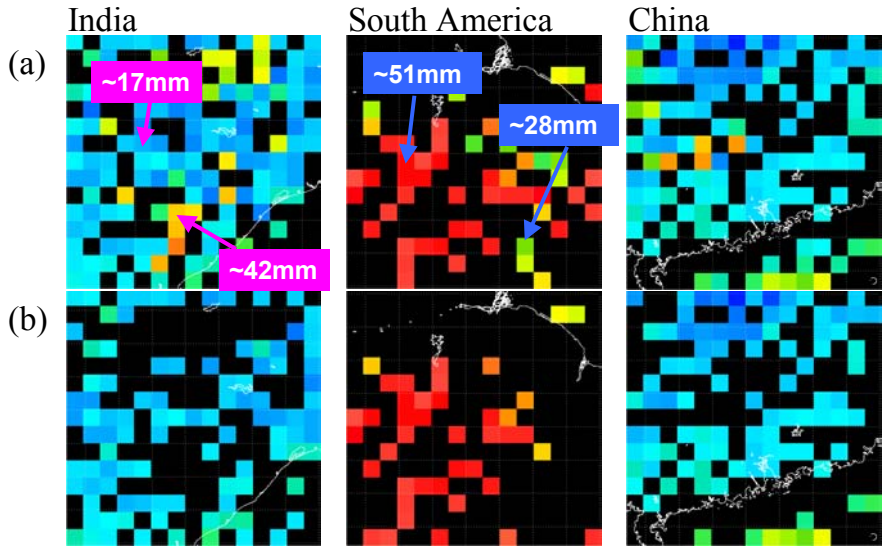

Figure 19. **ATOVS Quality Control example. Sample image of January 1, 2000 ATOVS TCWV (a) before and (b) after noise filtering process. An average of 8000 points/day get screened out (approximately 6%–8%). These noise points have an average value 20 mm different than surrounding points.**

ATOVS are known to have questionable results in upper levels (above 300 mb; Reale, 2001), with excessively high values over high latitude regions. NESDIS did not correct this problem until 2002. To

prevent bad data being merged into our product, the ATOVS 200 mb mixing ratio field and 200–300 mb precipitable water field are not used in NVAP-NG.

- Pathfinder PATH A dataset 5° x 4° artifact

An artifact of 5 x 4 degree grid boxes stands out in the monthly average field from Pathfinder data. Figure 20a shows the original Pathfinder Path A TCWV field. Note the "boxy" pattern in the data, which should not be apparent since it is on a 1-degree grid. Upon reviewing the literature on the Pathfinder Path A dataset (Susskind et al., 1997), it was discovered that the TOVS retrievals in Pathfinder use a first guess from a GCM (Goddard GEOS-1 model). The GCM was run at a 5° x 4° spatial resolution. In order to reduce this effect and still use the dataset, we devised a method to remove some data points from the original grid. Roughly 2 percent of the total data amount was removed. Figure 20b is a map of the points that were removed. Points are selected from the most outer points from the center of each 5° x 4° grid, as demonstrated by the gray boxes in Figure 20c. We removed the corners of each 5° x 4° grid box. This method is being used mainly over the land because the effect of the model first guess is more apparent over land, owing to higher natural variability due to effects like mountains and coastlines. Figure 20d shows the result of applying the Pathfinder Path A artifact reduction method to the final merged product. Note that the "blocky" pattern seen in Figure 20a has been greatly reduced.

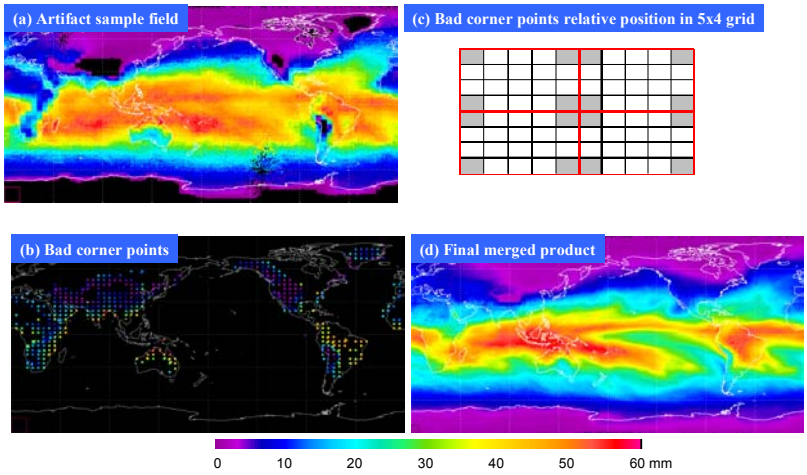

Figure 20. Pathfinder Path A 5x4 degree artifact. (a) January 2000 monthly average 850–1000 mb Pathfinder PW shows an example of the 5°x4° artifact (blockiness, particularly over land such as Africa and South America). (b) A map of Path A points that will be removed from the dataset. (c) Showing relative position of the points to be removed (gray boxes) corresponding to the 5°x4° grid. (d) Final merged monthly average TCWV product for January 2000 after minimizing the artifact. Notice the improvement over panel (a) over land.

In addition, the median-type filtering method used for ATOVS is being applied to the Path A dataset to reduce isolated high or low points.

- Quality control in merge procedure

After merging all the datasets together, a maximum threshold is set according to different output product types in the final merge routine. Table 5 is the list of values used to eliminate unreasonable data values. These points are mainly caused by individually poor retrieval results. The final quality control check seeks to find outlying points within a grid box and large gradients between adjacent grid boxes. The standard deviation of the points within the grid box is calculated, and points greater than two standard deviations from the mean are rejected. Finally, individual values are compared to the mean values in adjacent eight grid boxes, and those whose values are outside a specified range are rejected from the grid box.

Table 5. Maximum Threshold Used for Each Output Product

	TCWV		Layered PW		Level q	
THRESHOLD USED FOR MAXIMUM VALUE	Input data type:		200-300 mb	0.4 mm	300 mb	0.9 g/kg
			300-500 mb	6.5 mm	500 mb	7.0 g/kg
	Microwave	80 mm	500-700 mb	16.0 mm	700 mb	14.0 g/kg
	Infrared	70 mm	700-850 mb	22.0 mm	850 mb	25.0 g/kg
			850-1000 mb	36.0 mm	1000 mb	40.0 g/kg

6.2 EXTERNAL PRODUCT INTERCOMPARISON

Within the Pathfinder project of NASA and during the NVAP to NVAP-NG transition a limited number of water vapor data product comparisons were completed. Simpson et al. (2001) compared the NVAP data from 1988 to 1995 to TOPEX / POSEIDON microwave radiometer (TMR) TCWV retrievals and ECMWF reanalysis fields. They found that NVAP was drier than TMW, which was in turn drier than ECMWF fields. It was determined that NVAP has sufficient relative accuracy for variability studies, although its absolute accuracy is uncertain. A reanalysis effort for NVAP was recommended to eliminate time-dependent biases. These biases are detailed in Appendix D.

Suggs and Jedlovec (2001) explored the time-dependent biases of the NVAP dataset through 1995. They concluded, in accordance with Simpson et al. (2001), that the discontinuity at the beginning of 1993 stemming from the use of the 22 GHz SSM/I channel should be addressed. The TOVS component of NVAP from 1990 to 1993 appears to introduce a dry bias with respect to collocated radiosonde measurements.

We performed our own intercomparison of NVAP using a "bridge" concept. November and December 1999 were chosen as bridge months. This means that NVAP was produced by the method Randel et al. (1996) used to create the 1988–1999 dataset and by our NVAP-NG techniques described here. Technically, 1998 and 1999 were a part of this project as well, but they were produced using heritage methods. The goal of the bridge effort was to look for systematic differences between the two approaches and provide a measure of the uncertainty of NVAP-NG.

The monthly means for the bridge months are shown in Figure 21. It is noted in all cases (stratified by hemisphere and oceans) that NVAP-NG is moister than the NVAP result by amounts less than 1 mm, or about 4 percent. We estimate that about 0.5 mm of this is due to the new SSM/I antenna pattern correction applied in NVAP-NG. It should be noted that how the NVAP-NG results are averaged down to the NVAP daily, 1-degree resolution can have a small effect on the results as well. In this case, a sampling technique was used.

		N.HEMIS	S.HEMIS	GLOBAL	GLOBAL-OCEAN ONLY
November 1999	NVAP-NG	23.57	23.59	23.58	25.87
	NVAP	22.90	22.86	22.88	25.05
December 1999	NVAP-NG	20.73	25.69	23.20	25.81
	NVAP	20.30	25.27	22.79	25.03

Figure 21. NVAP vs. NVAP-NG bridge month comparison. Results of global average from NVAP and NVAP-NG. Note that the NVAP dataset is interpolated (averaged) from a 1-degree to a ½-degree grid for comparison. Further work will explore whether averaging or sampling is the best approach to this. NVAP-NG is generally moister than NVAP by 1 mm or less.

A graphical portrayal of the bridge month differences is shown in Figure 22a for December 1999. The NVAP-NG method is slightly moister over the oceans (green coloration). This is primarily due to the antenna pattern correction. NVAP-NG is drier in polar regions and mountainous regions in general. NVAP-NG tends to be drier over lower elevation land areas as well (blue coloration). The white areas, which are essentially the same, congregate in the midlatitude regions. A histogram of the differences is shown in Figure 22b. Most of the differences are 2 mm or less.

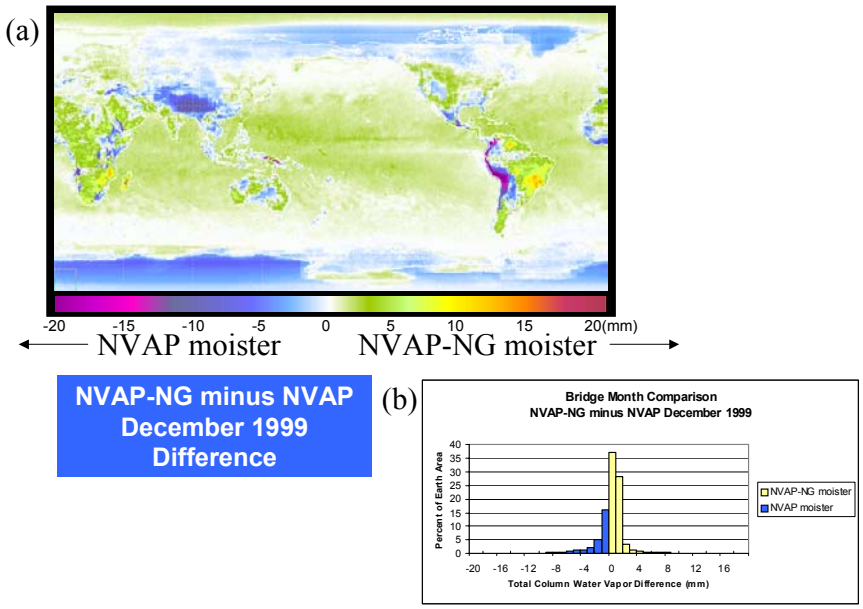

Figure 22. **NVAP vs. NVAP-NG bridge month comparison. (a) December 1999 total column water vapor difference created from NVAP-NG minus NVAP. (b) Histogram of differences. NVAP-NG tends to be moister over the tropical oceans and over non-mountainous land regions.**

7. SCIENTIFIC RESULTS AND DISCUSSION

We present here a sampling of scientific results developed at STC-*METSAT* during NVAP-NG. Further exploration of this new dataset is ongoing at this time (August 2003). A journal paper expanding on the NVAP-NG results is in preparation. The principal science questions addressed below and in several papers in preparation are outlined by Asrar et al. (2001). They are:

"How is the global cycling of water changing?"

"How well can long-term climatic trends be predicted or assessed?"

"What trends in atmospheric constituent are driving climate?"

"What is the natural variability of Earth's climate?"

7.1 GLOBAL AND MONTHLY MEANS

The global average of TCWV for each month of NVAP-NG is shown in Figure 23. The monthly average for January and July 2000 is also shown. Note that there is a high degree of agreement between the 2000 and 2001 monthly averages. They differ by only a few tenths of a millimeter at most. This is encouraging because it attests to the stability of the algorithms and instruments used in NVAP-NG. For instance, July 2000 had only NOAA-15 input, while July 2001 had both NOAA-15 and NOAA-16 input (refer back to Figure 3 for a view of the changing time coverage of the sensors). If there were unknown algorithm or calibration drifts, we might see a consistent difference between these two years.

(a)

Global Average		
	2000	2001
Jan	23.26	23.55
Feb	23.73	24.15
Mar	24.15	24.51
Apr	24.91	24.83
May	25.16	25.22
Jun	25.57	25.64
Jul	26.60	26.72
Aug	26.49	26.75
Sep	25.33	25.49
Oct	24.63	24.46
Nov	23.84	23.96
Dec	23.48	23.85

(b) Jan 2000 monthly average

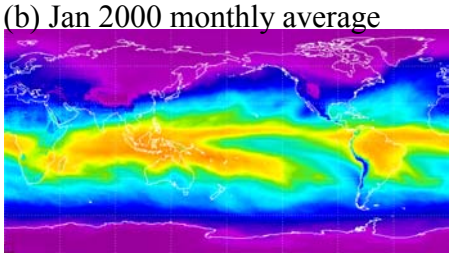

(c) July 2000 monthly average

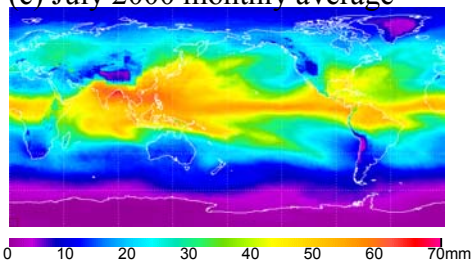

Figure 23. Sample NVAP-NG results. (a) Total column water vapor global average for each month. Monthly average field for (b) January 2000 (c) July 2000.

The January and July 2000 monthly mean plots in Figure 23 look realistic. NVAP-NG was created at ½-degree spatial resolution, in contrast to the 1-degree resolution used previously. We expect topographic boundaries to water vapor to be resolved better with NVAP-NG. The appearance of the Andes Mountains, the Tibetan Plateau, and the Rocky Mountains in Figures 23 b-c supports this notion.

The long-term mean TCWV amounts from NVAP and NVAP-NG are shown in Figure 24. The annual averages for each dataset by year are also shown. One difference in the two global plots is that NVAP-NG has more TCWV over land in moist tropical regions. The warm pool region over New Guinea and South America are examples. NVAP-NG appears to be drier over mountainous regions; the Tibetan Plateau is a good example. The hemispheric and global means for 2000 and 2001 compared to 1988–1999 reveals that, while 2000 and 2001 are two of the moister years, they are not outliers and are quite close to the previous 12 years. This is evidence that any biases in NVAP-NG are on the order of a millimeter or less.

(a) NVAP 1988 - 1999

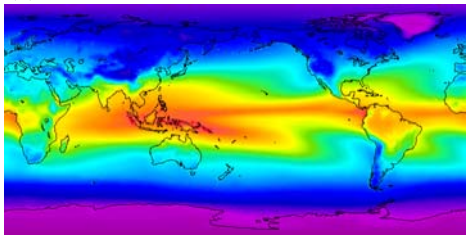

(b) NVAP-NG 2000 - 2001

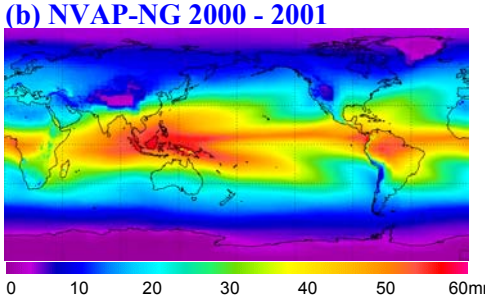

(c) Annual Averages (mm)

YEAR	N.HEMIS	S.HEMIS	GLOBAL
1988	26.24	23.76	25.00
1989	25.64	23.37	24.50
1990	25.83	23.21	24.52
1991	25.82	23.18	24.50
1992	24.87	23.27	24.07
1993	25.37	22.95	24.16
1994	25.72	22.86	24.29
1995	25.61	23.02	24.32
1996	25.39	22.74	24.06
1997	25.79	22.93	24.36
1998	25.95	23.85	24.90
1999	25.45	22.78	24.12
2000	**25.76**	**23.78**	**24.76**
2001	**25.89**	**23.98**	**24.93**

Figure 24. Results from the 14-year long-term global water vapor dataset. (a) NVAP (1988–1999) and (b) NVAP-NG (2000–2001) total column water vapor field and (c) Annual average values (NVAP-NG values shown in blue).

NVAP had fewer sources of vertical profile information than NVAP-NG (radiosondes and TOVS versus AMSU, ATOVS, SSM/T-2, and Pathfinder Path A). NVAP-NG performs less smoothing of the vertical structure via spatial interpolation than NVAP. During the development of NVAP-NG it was found that the AMSU and SSMT-2 retrievals were a bit drier at upper levels than ATOVS and Pathfinder. Since

AMSU and SSM/T-2 cannot currently perform retrievals over land, this should lead to increased gradients near coastlines. Figure 25 shows monthly averages of the layered precipitable water for five layers in January 2000.

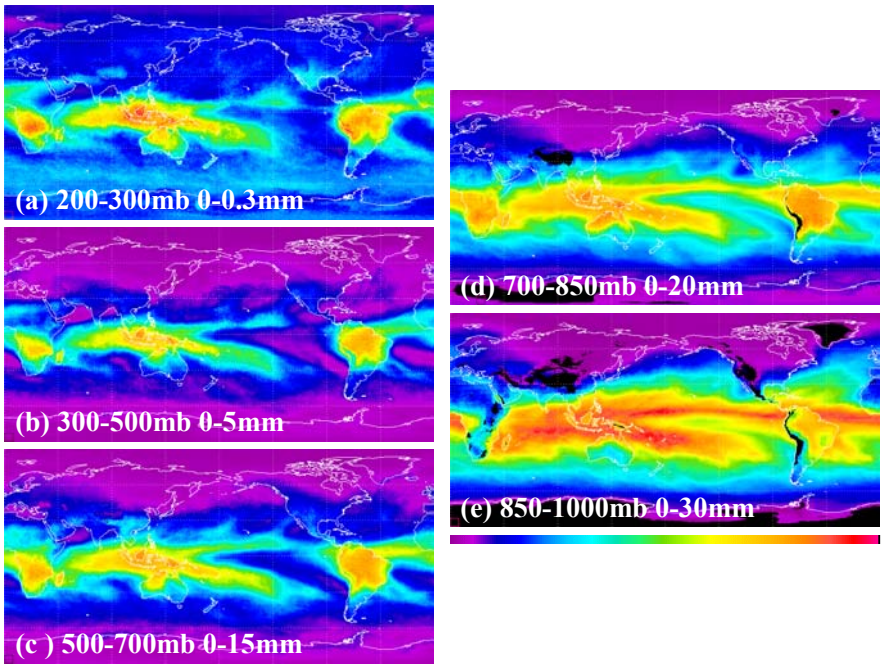

Figure 25. January 2000 monthly average layer precipitable water field for 5 layers (a–e).

Several features are noteworthy in Figure 25. First is the high degree of correlation between layers. This has been observed in the NVAP results as well. However, there are exceptions to this that might provide important information about atmospheric behavior. Note that the Intertropical Convergence Zone in the East Pacific is well defined at lower levels but appears more broken above 500 mb. While an exponential decay with height of layered water vapor content is in general a good assumption, Figure 25 reveals that there are regions where this is not true. The water vapor may decrease with height, but the rate at which this occurs can be quite geographically variable.

The expected higher gradient in water vapor near coastlines is apparent in a few regions in Figure 25. For instance, notice the reversal in water vapor gradient over Borneo by moving upwards through the vertical levels. A similar effect is visible along the northern coast of Australia.

7.2 LONG-TERM ANOMALY TREND

In Figure 26 we present the NVAP water vapor anomaly compared to Reynolds sea surface temperature anomaly. Our work with NVAP continues to extend this time series, and 1998 and 1999 are presented here. They show a downward trend of global water vapor of about 1 mm since the major El Nino of 1997–1998. We have not included 2000 and 2001 on Figure 26 at this time due to some additional work needed to normalize the anomalies to a common time period.

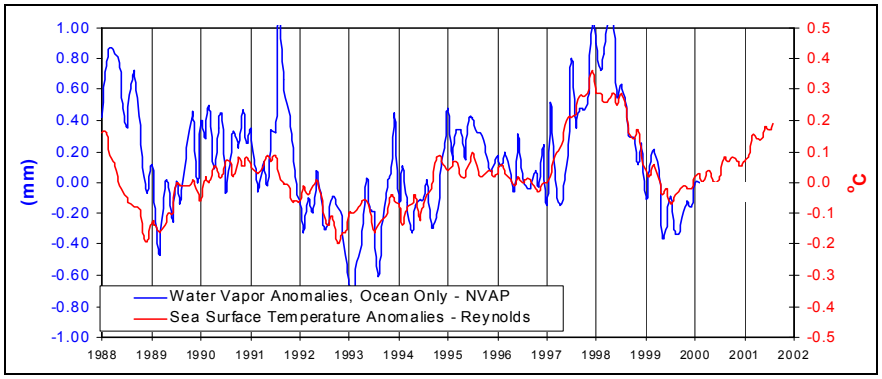

Figure 26. Comparison of sea surface temperature and total column water vapor anomalies from 1988 through 1999. Calculation of the NVAP-NG anomalies is in progress as of August 2003.

7.3 WATER VAPOR TRANSPORT VARIABILITY

Nearly half of the energy carried across the midlatitudes towards the poles is in the form of latent heat (Cohen et al., 2000). In this section, we combine winds from the NCEP reanalysis (Kalnay et al., 1996) with NVAP water vapor fields to examine the interannual variability of water vapor transport across the southern United States. Such variability has large sensible effects, such as the heavy rain and floods in California during the El Nino of 1997–1998 and greater rainfall across the southeast United States.

In this section, the moisture fluxes before and during the major El Nino of 1997–1998 are compared. We present the monthly mean moisture fluxes for July 1996 and January 1997 (pre-El Nino with weak La Niña conditions), and July 1997 and January 1998 (El Nino in progress). The fluxes are vertically integrated and calculated using the method of Cohen et al. (2000). A 12-year time series of flux variability across western and southern North America is also shown.

Figures 27 and 28 show the U (east-west) and V (north-south) flux components for the globe at 6-month intervals for July 1996 through January 1998. The calculation was not performed where the

topography was above the 700 mb surface. There is quite a bit of agreement between each year. The Indian monsoon is well defined in the V-field in July of both years, but is absent in January. The storm track regions to the east of the continents in the Northern Hemisphere are well defined in both the U and V fields. There is an intensified region of eastward moisture transport north of Australia in January 1998 as compared to January 1997.

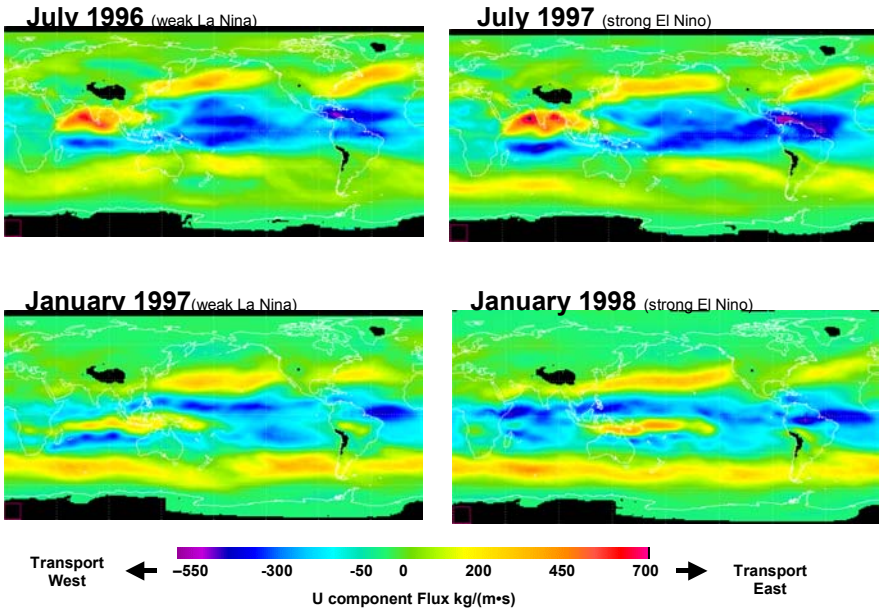

Figure 27. U (east-west) component of vertically integrated moisture flux for 4 months. July 1996 and January 1997 represent weak La Nina conditions, while July 1997 and January 1998 represent El Nino conditions.

A close-up view of transport around the U. S. region is shown in Figures 29 (U-component) and 30 (V-component). The U-component fields are quite similar between each January and July. This indicates that the El Nino in progress in January 1998 was not manifested by large zonal transport anomalies in water vapor. The V-component fields are quite different during these times though. There is a greater amount of northward transport from the Gulf of Mexico during January 1998 than during January 1997. The northward flux of moisture into the west coast is displaced further southward in January 1998, with greater fluxes closer to the coast. The July fields look quite similar between the two years.

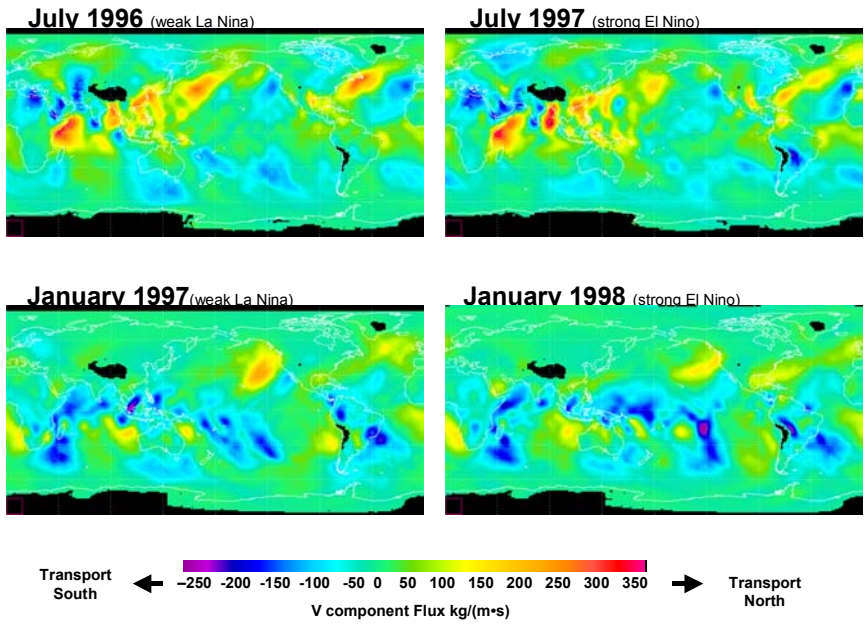

Figure 28. **V (north-south) component of vertically integrated moisture flux for 4 months. July 1996 and January 1997 represent weak La Nina conditions, while July 1997 and January 1998 represent El Nino conditions.**

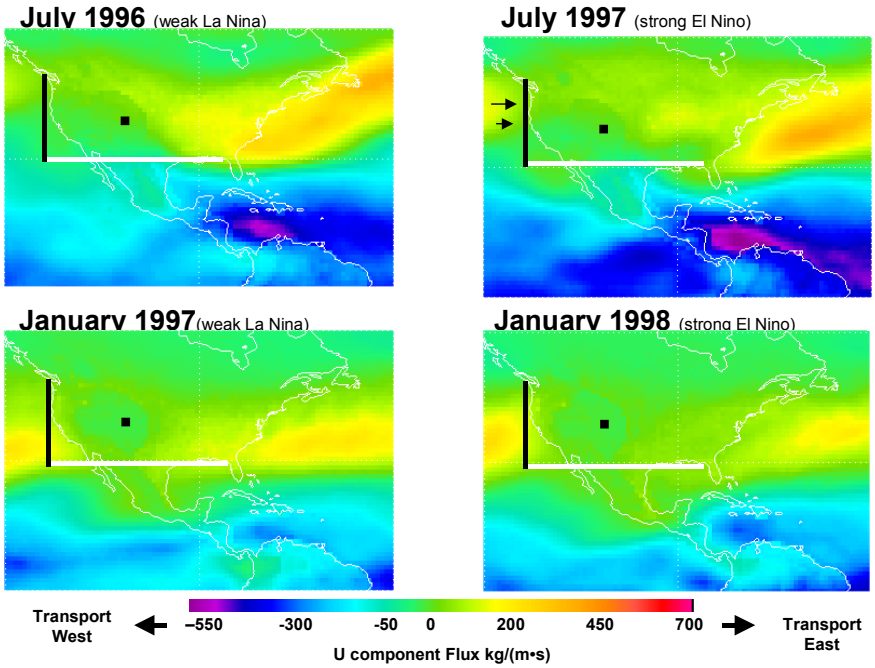

Figure 29. **U (east-west) component of vertically integrated moisture flux for 4 months over U.S.A. July 1996 and January 1997 represent weak La Nina conditions, while July 1997 and January 1998 represent El Nino conditions.**

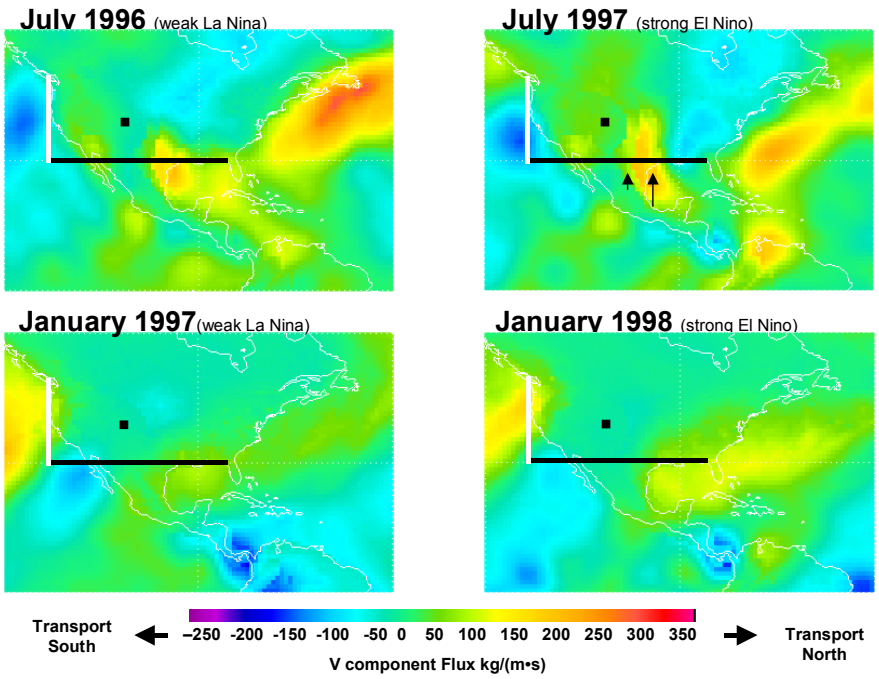

Figure 30. V (north-south) component of vertically integrated moisture flux for 4 months over U.S.A. July 1996 and January 1997 represent weak La Nina conditions, while July 1997 and January 1998 represent El Nino conditions. Black and white lines are used to calculate flux across those boundaries.

Figure 31 shows a time series for 1988–1999 of the U- and V-fluxes across the two lines shown in Figure 30 (southern and western United States). The multivariate ENSO index, with El Nino conditions indicated by red shading, is shown in Figure 31a for the same time period. An annual cycle is apparent in each field, although its magnitude is quite variable. It is interesting to look at phase and magnitude of the U- and V-components. In the fall of 1993, the V-component flux reaches a peak while the U-component flux is at a minimum. This implies a high-amplitude circulation pattern at this time. The type of plot shown in Figure 31 is a new use of the NVAP data and would be a useful tool to classify circulation regimes in a region. Perhaps this type of figure for a region would have some seasonal predictive ability?

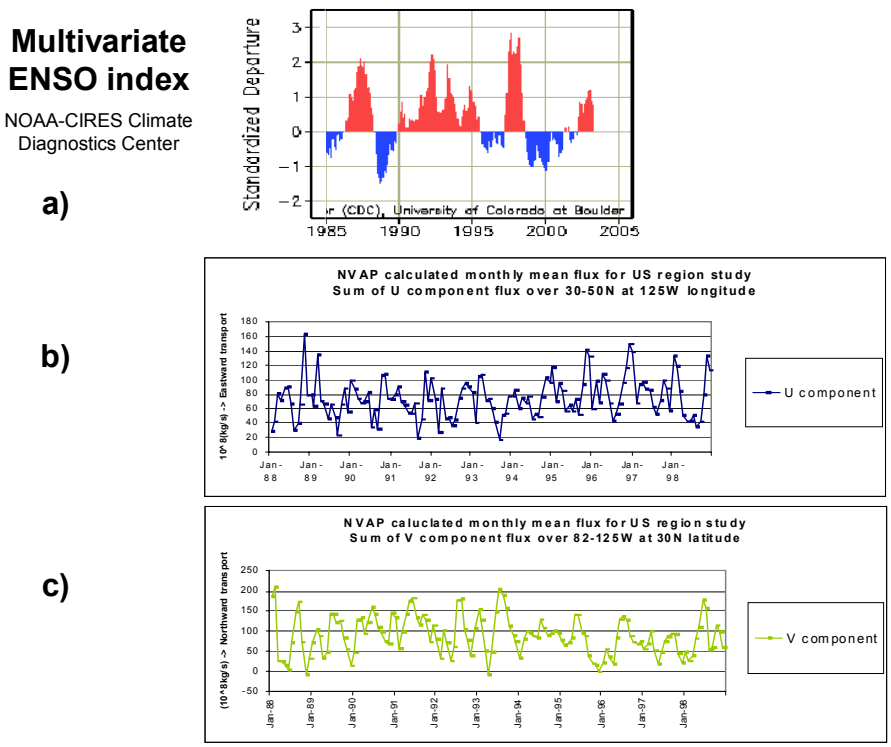

Figure 31. Multivariate ENSO Index from CDC (a) and U-component of vertically integrated moisture flux (b) and V-component (c) across boundaries in Figure 30. Time series of flux is from January 1988 to December 1999.

SUMMARY

STC-*METSAT* has added four more valuable years of the NVAP Climate Data Record (CDR) to the NASA DAAC system. Scientific demand for this unique dataset remains high. NVAP has been brought into the 21st century with advanced algorithms and sensor inputs. By all measures, the spatial and temporal resolution of NVAP has been increased. The multitude of sensors used will allow an improved specification of error bars on NVAP. However, we still have not reached an original goal of having a significant overlap period of the NVAP CDR with the water vapor measurements from NASA's Aqua satellite, which began producing products in mid 2002.

Future possibilities we will propose with NVAP involve extending into the era of hyperspectral instruments such as the AIRS instrument on NASA's Aqua platform. The AMSR instrument on Aqua is also well suited for further exploration. Connecting NVAP results with NPOESS-era instruments will create the multi-decadal time series needed to detect signals of global change. A reanalysis cycle may be useful at some point to enhance the ability of NVAP to detect decadal-scale regional and global trends. In preparation for this possibility—recommended by the user science community—we have prepared Appendix D.

REFERENCES

Asrar, G. J., A. Kaye, and P. Morel, 2001: NASA research strategy for earth system science: Climate component. *Bull. Amer. Meteor. Soc,* 82, 309-1329.

Atkinson, N. C., 2001: Calibration, monitoring and validation of AMSU-B. *Adv. Space Res.,* 28/1, 17-126.

Cohen, J. L., D. A. Salstein, and R. D. Rosen, 2000: Interannual variability in the meridional transport of water vapor. *Jour. Hydrometeorology,* 1, 547-553.

Colton, M. C. and G. A. Poe, 1999: Intersensor calibration of DMSP SSM/I's: F-8 to F14, 1987–1997. *IEEE Trans on Geosci. and Rem. Sens.,* 37/1, 418-439.

Engelen, R. J. and G. L. Stephens, 1998: Characterization of Water Vapour Retrievals from TOVS/HIRS and SSM/T-2 Measurements. *Quart. J. Roy. Met. Soc.,* 125/553, 331-351.

Forsythe, J. M., D. L. Randel, S. Woo, D. S. McKague, and T. H. Vonder Haar, 2003: Extending the 12-year NVAP global water vapor dataset into the 21st century. Preprints, 12th AMS Conference on Satellite Meteorology and Oceanography, Long Beach, California, Feb. 2003.

Greenwald, T. J., G. L. Stephens, T. H. Vonder Haar, and D. L. Jackson, 1993: A physical retrieval of cloud liquid water over the global oceans using SSM/I observations. *J. Geophys. Res.,* 98, 18471-18488.

Grody, N.C., 1991: Classification of snow cover and precipitation using the Special Sensor Microwave/Imager (SSM/I). *J. Geophys. Res.,* 96, 7423-7435.

Huffman, G. J., R. F. Adler, B. Rudolf, U. Schneider and P. R. Keehn, 1995: Global precipitation estimates based on a technique for combining satellite-based estimates, rain gauge analysis, and NWP model precipitation information. *J. Climate*, 8, 1284-1295.

Kalnay, E., M. Kanamitsu, R. Kistler, W. Collins, D. Deaven, L. Gandin, M. Iredell, S. Saha, G. White, J. Woollen, Y. Zhu, M. Chelliah, W. Ebisuzaki, W. Higgins, J. Janowiak, K. C. Mo, C. Ropelewski, J. Wang, A. Leetsmaa, R. Reynolds, Roy Jenne, and Dennis Joseph, 1996: The NCEP/NCAR 40-year reanalysis project. *Bull. Amer. Meteor. Soc,* 77, 437-471.

Kidder, S. Q., M. D. Goldberg, R. M. Zehr, M. DeMaria, J. F. W. Purdom, C. S. Velden, N. C. Grody, S. J.

Kusselson, 2000: Satellite Analysis of Tropical Cyclones Using the Advanced Microwave Sounding Unit (AMSU) *Bull. Amer. Meteor. Soc,* 81/6, 1241-1259.

Koch, S. E., M. Desjardins, and Paul J. Kocin, 1983: An Interactive Barnes Objective Map Analysis Scheme for Use with Satellite and Conventional Data. *J. Climate and Applied Meteorology,* 22, 1487-1502.

McKague, D. S., R. J. Engelen, J. M. Forsythe, S. Q. Kidder, and T. H. Vonder Haar, 2001: An optimal-estimation approach for water vapor profiling using AMSU. 11th AMS Conference on Satellite Meteorology and Oceanography, Madison, Wisconsin.

Randel, D. L., T. H. Vonder Haar, M. A. Ringerud, G. L. Stephens, T. J. Greenwald, and C. L. Combs, 1996: A New Global Water Vapor Dataset. *Bull. Amer. Meteor. Soc,* 77, 1233-1246.

Reale, A. L, 2001: NOAA Operational Sounding Products from Advanced-TOVS Polar orbiting Environmental Satellites. NESDIS Technical Report 102.

Reynolds, R. W., N. A. Rayner, T. M. Smith, D. C. Strokes, and W. Wang, 2002: An improved in situ and satellite SST analysis for climate. *J. Climate,* 15, 1609-1625.

Ross, R. J., W. P. Elliott, and D. J. Seidel, with Participating AMIP-II Modeling Groups, 2002: Lower-Tropospheric Humidity—Temperature Relationships in Radiosonde Observations and Atmospheric General Circulation Models. *Jour. of Hydrometeorology,* Vol. 3, No. 1, pp. 26–38.

Simpson, J. J., J. S. Berg, C. J. Koblinsky, G. L. Hufford, and B. Beckley, 2001: The NVAP global water vapor dataset: Independent cross-comparison and multiyear variability. *Remote Sensing of Environment*, 76, 112-129.

Susskind, J., P. Piraino, L. Rokke, L. Iredell, and A. Mehta, 1997: Characteristics of the TOVS Pathfinder Path A Dataset. *Bull. Amer. Meteor. Soc.,* 78/7, 1449-1472.

Suggs, R. J. and G. J. Jedlovec, 2001: Internal consistency of the NVAP water vapor dataset. 11th AMS Conference on Satellite Meteorology and Oceanography, Madison, Wisconsin.

Vonder Haar, T. H., J. M. Forsythe, D. L. Randel, and S. Woo, 2003: Analysis of the NVAP water vapor dataset: A tool for monitoring Earth's water vapor from daily to decadal scales. Preprints, 12th AMS Conference on Satellite Meteorology and Oceanography, Long Beach, California, Feb. 2003.

Vonder Haar, T. H., D. L. Reinke, D. L. Randel, G. L. Stephens, C. L. Combs, and T. J. Greenwald, 1995:

Production of a long-term global water vapor and liquid water data set using ultra-fast methods to assimilate multi-satellite and radiosonde observations. STC Technical Report 2927. Final Report, NASA Contract NASW-4715. 24 pp. Science and Technology Corporation, Hampton, Virginia.

APPENDIX A. NVAP-NG DATA PRODUCT AND FILE NAMING CONVERSIONS

Gridded Product	12 hour	Daily	Monthly	Annual
Blended Total PW (precipitable water)	A	F	J	K
Blended 5 Layer PW	AA	FF	JJ	KK
Blended 6 Level q	AAA	FFF	JJJ	KKK
Data Source for Total PW	B	G		
Data Source for Layer PW	BB	GG		
Data Source for Level q	BBB	GGG		
Total PWC statistic	C			
Layer PWC statistic	CC			
Level q statistic	CCC			
Blended LWP (liquid water path)	D	H		
Blended CLW (cloud liquid water)	E	I		

Filename format Archive Data Set

A: YYYYMM_wv12.tc
B: YYYYMM_ds12.tc
C: YYYY_DDD-DDDstat.tc
D: YYYY_DDD-DDDlw12.tc
E: YYYY_DDD-DDDcw12.tc
F: YYYYMM_wv24.tc
G: YYYYMM_ds24.tc
H: YYYY_DDD-DDDlw24.tc
I: YYYY_DDD-DDDcw24.tc
J: YYYYwv.tcmave
K: YYYYwv.tcyave
AA: YYYYMM_wv12.pot
BB: YYYYMM_ds12.pot
CC: YYYY_DDD-DDDstat.lpw
FF: YYYYMM_wv24.pot
GG: YYYYMM_ds24.pot
JJ: YYYYwv.potmave
KK: YYYYwv.potyave
AAA: YYYYMM_sph12.q
BBB: YYYYMM_ds12.q
CCC: YYYY_DDD-DDDstat.q
FFF: YYYYMM_sph24.q
GGG: YYYYMM_ds24.q
JJJ: YYYYsph.qmave
KKK: YYYYsph.qyave

Note		12 hour	Daily
C	Data POPulation	V	V
CC	Data POP at 500-700mb layer only	V	V
CCC	Data POP at 500mb level only	V	V
C	Data range	V	
CC	Data range info for all layer	V	
CCC	Data range info for all level	V	

YYYY = 4 digit year (e.g. 2000)

MM = month (e.g. 01 for Jan)

DDD = Julian day (e.g. 001 for Jan 1st)

Start/end Julian day for 1st/2nd set of DDD

mave = monthly average

yave = annual average

wv = water vapor

pot = percent of total

sph = specific humidity

lw = liquid water path

cw = cloud liquid water

ds = data source code

APPENDIX B. DATA SOURCE BIT CODES (1 = LSB, ON MEANS HAS THAT INPUT)

Number of bits = 16

(1) = 'DSB SSM/I Leftovers'
(2) = 'DSB SSM/I Sat 1'
(3) = 'DSB SSM/I Sat 2'
(4) = 'DSB SSM/I Sat 3'
(5) = 'DSB Pathfinder Path A TOVS'
(6) = 'DSB ATOVS N15'
(7) = 'DSB ATOVS N16'
(8) = 'DSB SSM/T2 Sat 1'
(9) = 'DSB SSM/T2 Sat 2'
(10) = 'DSB AMSUB N15'
(11) = 'DSB AMSUB N16'
(12) = 'DSB TMI TRMM'
(13) = 'TOPOGRAPHICALLY REMOVED'
(14) = 'SPATIAL INTERPOLATED'
(15) = 'TEMPORAL INTERPOLATED'
(16) = 'MISSING'

APPENDIX C: DATA AVAILABILITY, THROUGHPUT AND SYSTEM DESCRIPTION

Table C1. Data Distribution (shading indicates data used)

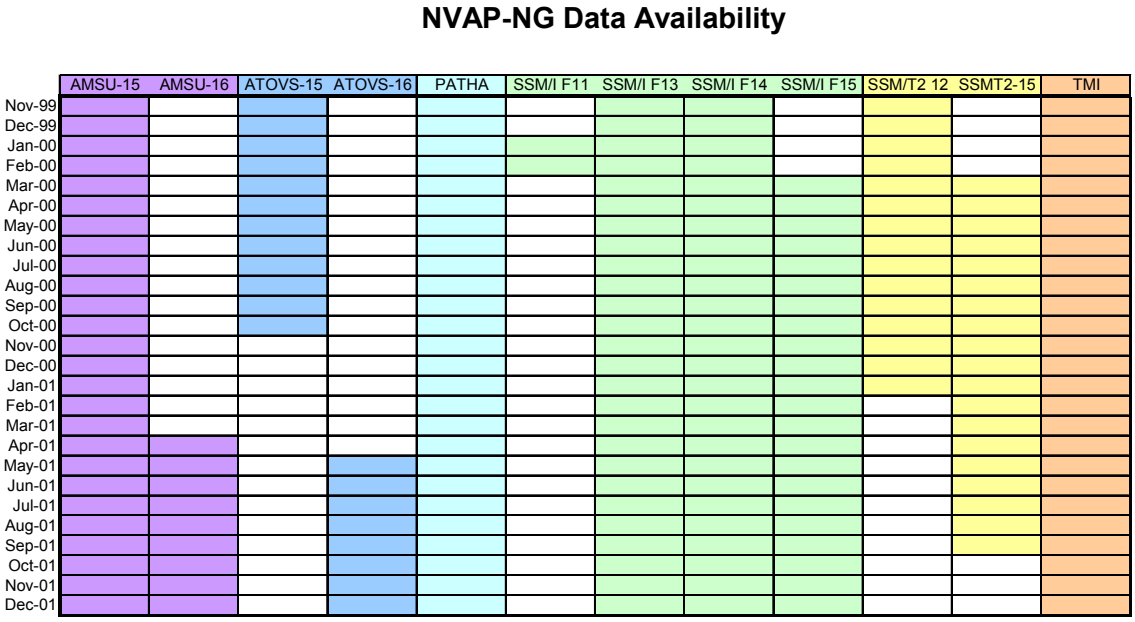

Table C2. System Throughput

SATELLITE	INPUT		OUTPUT	
	MONTHLY	TOTAL	MONTHLY	TOTAL PRODUCT
SSMI (F11/F13/F14/F15)	600 MB	42.5 GB	TCWV/DSB 90 MB CLW/LWP 90 MB STATISTIC 105 MB	6.5 GB
TMI	350 MB	9.0 GB		
ATOVS (N15/N16)	200 MB	3.5 GB	5 Layered PW 230 MB DSB 230 MB STATISTIC 200 MB	16.5 GB
PATH A TOVS	150 MB	4.0 GB		
AMSU (N15/N16)	650 MB	21.5 GB	6 Level Q 280 MB DSB 280 MB STATISTIC 230 MB	18.5 GB
SSM/T2 (F12/F15)	550 MB	15.0 GB		

Table C2. Computer Systems Used in NVAP-NG Project (Windows 2000, Compaq Visual Fortran v6.5, IDL v 5.4)

System Name	Arches	Zion	Kirk	Riker	Adhara	Suhail
# of Disk	1	2	2	2	2	2
Amount of Space/Disk	150 GB	80 GB	80 GB	38 GB	143 GB	143 GB
Processor	Pentium 4	Pentium 4	Pentium 4	Pentium 3	Pentium 4	Pentium 4
CPU	1700 MHz	1700 MHz	2.53 GHz	600 MHz	1400 MHz	1400 MHz
RAM	1 GB	532 MB	1 GB	785 MB	532 MB	532 MB
Main Usage	Software develop / Process merge	Process merge / QC	Run OE retrieval / Process merge	Software develop / QC	Run OE retrieval / input data process	Run OE retrieval / input data process

APPENDIX D: SUMMARY OF NVAP TIME-DEPENDENT BIASES (1988–1999)

ITEM		TIME AFFECTED	DOCUMENTATION	DETAILS	ESTIMATED EFFECT	COMMENTS
1.	Operational TOVS values < 1 mm not merged.	Jan. 1, 1988–Dec. 31, 1995. New TOVS source (Soden) began Jan. 1, 1996 and removed issue.	Internal	Both total and 3-layer product affected.	May give slight (<< 1 mm) dry bias to global results before 1996. Polewards of 60°N main influence.	Values before 1996 came as integers; a conscious decision to mark as missing = 0
2.	Number of operational TOVS soundings.	1988–1993: 15 K/day max from all NOAA platforms. 1994: Increased to 25 K/day max.	Internal; NOAA Users Guide	NOAA operational constraint.	Unknown. More spatial resolution. Perhaps more soundings closer to cloudy regions, therefore moister?	
3.	Radiosonde quality control	1988–1999; 1988–1992	Ross et al., 2002	Manual (visual) QC applied 1988–1992. In 1993, began automated NVAP climatological QC of TPW based on 5-year mean (refuse points 1–4 σ outside mean).	Beginning 1993, 2%–3% fewer radiosonde points used. Since erroneous values typically high, may give moist bias pre-1993.	STC did not receive profiles, 5 layer PW twice/day received.
4.	Radiosonde plotting error	1988–1992	N/A	Southern hemisphere radiosondes plotted one degree too far north. Repaired Jan. 1, 1993.	Negligible, may have some effect on climatology near radiosonde stations.	Pure programming bug.

ITEM		TIME AFFECTED	DOCUMENTATION	DETAILS	ESTIMATED EFFECT	COMMENTS
5.	Land mask adjustments (SSM/I)	Post-1992: 1993—Many more points added to land mask 1994–1997, 10–20 added per year 1998–1999: ¼-degree landmask and 5 x 5 filter	Internal	Mask allowed retrievals near coastlines, allowing large TBs into retrieval. In 1998, moved to Wentz's ¼-degree landmask and a 5 x 5 filter.	Moist SSM/I bias pre-1993. Magnitude unknown.	
6.	Precipitation test (SSM/I)	1988–1992	Greenwald et al., 1993, 1995	January 1993, began using Grody's (1991) SSM/I precipitation test.	Negligible	
7.	Sea ice detection (SSM/I)	1988–1992	Internal	1988–1992, used subroutine in Greenwald's code; 1993, began statistical check on SSM/I TPW, outliers removed.	Moist bias pre-1993 in polar ice regions. Magnitude unknown.	

ITEM		TIME AFFECTED	DOCUMENTATION	DETAILS	ESTIMATED EFFECT	COMMENTS
8.	SSM/I use of 22 GHz	1988–1992	Greenwald et al., 1993, 1995	***Look at paper for threshold and Greenwald analysis.*** PWC > 53.4 mm: use 19, 22, and 37 GHz PWC < 53.4 mm: use 22 GHz and 37 GHz	30°N–30°S doesn't change; dry bias overall, but what is TOVS and what is SSM/I? Moist bias 1988–1992 in low TPW regions (Suggs and Jedlovec, 2001: could also be better ice and precip. tests).	Reported in Simpson et al., 2001.
9.	SSM/I source and Greenwald offset	1988–1999: Impact varies according to number/identifica-tion of SSM/I in use.	Greenwald et al, 1993, 1995; Suggs and Jedlovec, 2001	January 1995 stopped normalization to F-8, thus F-13 & F14 PWC artificially low.	***Significant (tenths of mm), impact depends on mix of SSM/I's at a given time.***	Wentz source for F-8, F-11, MSFC, FMNOC, NESDIS SSM/I sources. Consistency?
10.	Topography masking (TOVS and radiosondes)	1988–1992	Internal	No topo masking pre-1993. Masked out layers below surface post-1993.	High terrain regions (e.g., Himalayas) could have TPW values too high.	
11.	TOVS algorithm biases	Jan 1, 1990; others?	McKague et al., 2001 Suggs and Jedlovek, 2001	(2 mm drop in TOVS global avg; see Randel's plot; Jedlovec Fig. 4)	Dry bias overall due to avoiding clouds.	IS THIS WHAT SUGGS AND JEDLOVEC SEE?

References cited in this Appendix are provided in the Reference Section of the main report.

REPORT DOCUMENTATION PAGE

Form Approved

OMB No. 0704-0188

1. AGENCY USE ONLY *(Leave Blank)*	2. REPORT DATE	3. REPORT TYPE AND DATES COVERED
	October 2003	Final Report—14 August 2000–13 August 2003

4. TITLE AND SUBTITLE
Continuation of the NVAP Global Water Vapor Data Sets for Pathfinder Science Analysis

5. FUNDING NUMBERS

Contract No. NASW-00032

6. AUTHOR(S)
Thomas H. Vonder Haar
John M. Forsythe
Darren McKague
David L. Randel
Benjamin C. Ruston
Shannon Woo

7. PERFORMING ORGANIZATION NAME(S) AND ADDRESS(ES)
Science and Technology Corporation
10 Basil Sawyer Drive
Hampton, VA 23666–1393

8. PERFORMING ORGANIZATION REPORT NUMBER

STC Technical Report 3333

9. SPONSORING/MONITORING AGENCY NAME(S) AND ADDRESS(ES)
NASA Goddard Space Flight Center
Greenbelt, MD

10. SPONSORING/MONITORING AGENCY REPORT NUMBER

11. SUPPLEMENTARY NOTES

12a. DISTRIBUTION/AVAILABILITY STATEMENT

12b. DISTRIBUTION CODE

13. ABSTRACT *(Maximum 200 words)*

The NASA Pathfinder water vapor project (NVAP) is a global, daily, 4-layer, satellite-derived water vapor dataset that covered the time period from 1988–1999. This effort extends NVAP into data years 2000 and 2001 with increased spatial and temporal resolution via a new suite of polar-orbiting satellite sensors. NVAP presents the longest (14 years), multi-layer Climate Data Record (CDR) available for scientific analyses. NVAP plays a key role in addressing crucial Earth science questions such as "How are global precipitation, evaporation, and the cycling of water changing?" "What trends in atmospheric constituents and solar radiation are driving global climate?" and "How well can long-term climatic trends be assessed or predicted?"

This phase of NVAP incorporated additional sensors not available in previous versions of NVAP. These include operational ATOVS soundings and microwave-only retrievals from AMSU and SSM/T-2, TMI retrievals, and TOVS Pathfinder soundings. Heritage SSM/I precipitable water and cloud liquid water retrievals are included. In a departure from NVAP 1988–1999, radiosondes were omitted. The retrieval results have been blended to produce a global, 50 km resolution, twice-daily water vapor product for July 1999–June 2001. Total column precipitable water and cloud liquid water are reported at each grid box. Layered precipitable water and mixing ratio are produced for layers at 1000–850, 850–700, 700–500, 500–300, and < 300 mb. Extensive diagnostics on source identification, number of samples and range of data are archived as well. Special emphasis was given to data quality control and SSM/I intercalibration.

In order to explore the consistency of NVAP pre- and post- 2000, November and December 1999 products were created using each approach to form a "bridge" comparison. Results indicate that the 2000–2001 NVAP products are slightly moister in the boundary layer and in a global total column sense by about 0.7 mm.

Water vapor transport variability into the United States was calculated and showed substantial interannual variability. Updated time series of water vapor anomalies compared to SST and tropospheric temperature anomalies were created as well and show generally good correlation.

The two new years of NVAP have been delivered to the NASA Langley DAAC and are available at http://eosweb.larc.nasa.gov/PRODOCS/nvap/tablenvap.html. A new CD-ROM showing animations and results from NVAP 1988–1999 has been created and is available from the GEWEX Project Office.

14. SUBJECT TERMS
NVAP; GEWEX; Pathfinder; precipitable water, cloud liquid water; water vapor profiles; satellite measurements of climate; climate monitoring; water vapor transport; water vapor feedback; AMSU; TMI; SSM/T-2; HIRS.

15. NUMBER OF PAGES
43

16. PRICE CODE

17. SECURITY CLASSIFICATION OF REPORT	18. SECURITY CLASSIFICATION OF THIS PAGE	19. SECURITY CLASSIFICATION OF ABSTRACT	20. LIMITATION OF ABSTRACT
Unclassified	Unclassified	Unclassified	SAR